1968

Molecular structure of gaseous hydrogen fluoride polymers and of the vapors of the seel complexes

Jay Janzen
Iowa State University

69-9865

JANZEN, Jay, 1940-

MOLECULAR STRUCTURE OF GASEOUS HYDROGEN FLUORIDE POLYMERS AND OF THE VAPORS OF THE SEEL COMPLEXES.

Iowa State University, Ph.D., 1968
Chemistry, physical

University Microfilms, Inc., Ann Arbor, Michigan

MOLECULAR STRUCTURE OF GASEOUS HYDROGEN FLUORIDE POLYMERS AND OF THE VAPORS OF THE SEEL COMPLEXES

by

Jay Janzen

A Dissertation Submitted to the

Graduate Faculty in Partial Fulfillment of

The Requirements for the Degree of

DOCTOR OF PHILOSOPHY

Major Subject: Physical Chemistry

Approved:

Signature was redacted for privacy.

In Charge of Major Work

Signature was redacted for privacy.

Head of Major Department

Signature was redacted for privacy.

Dean of Graduate College

Iowa State University
Of Science and Technology
Ames, Iowa

1968

TABLE OF CONTENTS

MOLECULAR STRUCTURE OF GASEOUS HYDROGEN FLUORIDE POLYMERS

Introduction

The hydrogen fluoride system is of basic interest in the study of strong hydrogen bonds, but there has remained uncertainty about the structures of the polymer species formed in the vapor. Because investigations by various methods, including an early visual electron diffraction study, have not yet led to agreement on the nature of the $(HF)_x$ oligomers, it seemed worthwhile to re-examine the vapors of hydrogen fluoride by modern high-precision electron diffraction, which is well suited to the study of geometries of gaseous molecules in the pressure range of appreciable HF polymer formation. This chapter describes the experimental conditions, analysis of data, and results of HF studies conducted at nominal temperatures of -19 and +22 °C. The conclusions are compared with inferences based on data from other sources.

Previous Work

Anomalous physical properties attributable to oligomer formation in hydrogen fluoride vapor have been the subject of numerous experimental measurements (1-18) since 1881, when Mallet (1) discovered that at 30 °C and 745 torr the vapor density is about twice that expected for HF monomer. The available observations, however, have been interpreted (3-23) in terms of different models for self-association equilibria in the vapor, with the result that conflicting views concerning the masses and structures of the gaseous hydrogen-bonded aggregates persist. This state of uncertainty has been noted before by other authors (13,14,21,23). The purpose of this sec-

tion is to comment on some of the data in the literature and to emphasize that the model of Franck and Meyer (18), in which a cyclic hexamer predominates over dimer and trace quantities of $(HF)_{j>2}$ chains, provides a coherent account of the physical properties of HF vapor. From this model it is found that under the conditions of appreciable association to be sought in the electron diffraction experiments, polymer species other than the cyclic hexamer may be expected to contribute negligibly to the diffraction pattern.

1. General description of the vapor

It will be convenient to introduce the notation of this section by writing the chemical formula for a sample of pure hydrogen fluoride vapor at equilibrium as a general mixture:

$$a_1HF + a_2(HF)_2 + \ldots + a_j(HF)_j + \ldots + a_J(HF)_J$$

The a_j's are numbers of moles. Such a sample occupies a volume v, has density ρ, and exerts total pressure p not greater than the saturation vapor pressure p_s. The total mass is then ρv, and the composition is subject to the constraints

$$\sum_{j=1}^{J} ja_j = \rho v/20.01 \quad \text{and} \quad a_j \geq 0. \tag{1}$$

An association factor x equal to the average molecular weight divided by 20.01 g/mole may be defined as

$$x = \sum ja_j / \sum a_j. \tag{2}$$

If the mixture behaves as an ideal gas, then

$$\sum a_j = pv/RT, \tag{3}$$

which allows x to be determined experimentally as

$$x_\rho = \rho RT/20.01p. \qquad (4)$$

(The distinction between x and x_ρ will be retained for use in treating the vapor as a nonideal gas.) This ratio has been observed to reach values as large[1] as 4.3. It is also observed that x_ρ is a strongly increasing function of increasing pressure and of decreasing temperature; the dependence on p and T is to be explained in terms of some set of mobile equilibria among the various species present in the vapor.

Regardless of whether the species $(HF)_{j\geq 2}$ is formed by a series of stepwise additions of monomer with equilibrium at each step

$$(HF)_i + HF \underset{\leftarrow}{\overset{K_{i,i+1}}{\rightarrow}} (HF)_{i+1} \qquad i = 1,\ldots,j-1$$

or by a single j-fold association

$$jHF \underset{\leftarrow}{\overset{K_j}{\rightarrow}} (HF)_j,$$

the detailed composition of the mixture at equilibrium depends on the values of the equilibrium constants K_j which relate the monomer and polymer fugacities f_1 and f_j:

$$K_j = f_j/f_1^j = \prod_{i=1}^{j-1} K_{i,i+1}. \qquad (5)$$

---

[1]Considering only conditions of pressure and temperature well below the critical values $p_c = 64.0_7$ atm and $T_c = 188$ °C (16). At the critical point the ratio $\rho RT/20.01p$ has the value 8.56, but the ideal gas law certainly does not apply. Spalthoff and Franck (17, Tabelle 3) give a more realistic estimate of x in the vicinity of the critical point as approximately 2 (2.08 at $p/p_c = 0.86$ and $T/T_c = 0.98$). Extrapolation of the empirical Eq. 5 of Jarry and Davis (8) to 188 °C gives the similar result x = 2.04. It may be noted from Fig. 1 that the compressibility factor $p_cM/RT_c\rho_c$ for the critical HF fluid appears much less anomalous when reckoned assuming an average molecular weight M = 2×20.01 than when the monomer weight M = 20.01 g/mole is used.

Fig. 1. Compressibility factors at critical conditions

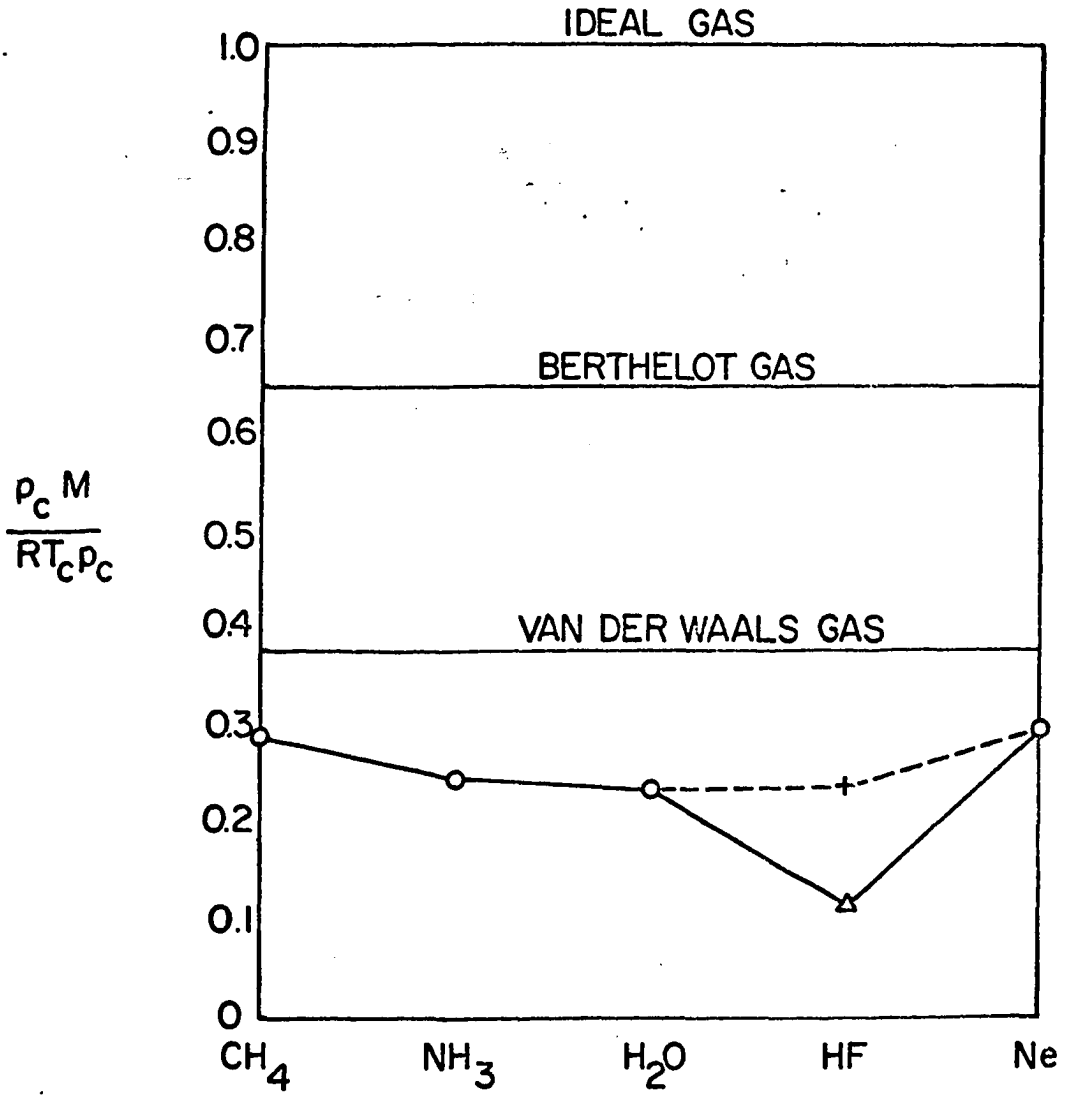
IDEAL GAS
1.0
0.9
0.8
0.7
BERTHELOT GAS
0.6
0.5
0.4
VAN DER WAALS GAS
0.3
0.2
0.1
0
$\frac{p_c M}{RT_c p_c}$
CH_4
NH_3
H_2O
HF
Ne
+ M = 2x20.01
△ M = 20.01

The problem is to identify which species exist in appreciable amounts. At sufficiently reduced pressure, x_ρ approaches unity, which is proof that monomer is the principal component under such conditions. Likewise, if x exceeds 4 there must be large contributions from species higher than tetramer. For a closer analysis, experiments of at least four different kinds must be considered as sources of relevant information concerning which species are negligible and which are not. Specifically, a description is sought which is in satisfactory accord with the available data on the following: vapor densities, not only at low pressures (9), but also under near-saturated conditions; thermal properties, including thermal conductivity (15), heat capacity (16-18), heat of vaporization (14), and entropy of association (14); infrared absorption band intensities (13,24); and dielectric polarization (12). Compatibility of such a description with electron diffraction data will be considered at length in a later section. In addition to data of the sorts just listed, there are also a few other, inconclusive observations to be discussed.

2. Vapor densities

Attention will first be given to the vapor density data available in the literature because it is in their interpretation that the most significantly disparate opinions have arisen.

For each species $(HF)_{j\geq 1}$ an ideal partial pressure P_j may be defined:

$$P_j = a_j RT/v. \tag{6}$$

The density of the mixture is then given by

$$\rho = (20.01/RT)\sum_j jP_j. \tag{7}$$

An isothermal series of vapor density measurements gives a finite set of

points (p,ρ) lying along some curve. The inferences to be drawn from such measurements depend on what sort of model specifying $\sum jP_j$ as a function of total pressure p is necessary to fit this curve. In the ideal gas approximation, $\sum jP_j$ is simply a polynomial in the monomer partial pressure P_1. But because in practice the observed data points are limited in number and contain experimental scatter, and because the number of terms in the sum $\sum jP_j$ used to fit them may be freely chosen, a unique answer cannot be obtained from density data. It is, rather, only possible to compare likely models with experiment, and perhaps to find the simplest model which will account for the data.

In the remainder of this section, the following special meaning will be attached to the word "model": A model will consist of an equation of state and a list of species $(HF)_j$ assumed to exist $(a_j > 0)$. By a "description" of HF vapor at some temperature will be meant a model, taken together with a set of numerical values for the parameters (equilibrium constants and nonideality constants, if any, needed to compute $\sum jP_j$ from the pressure p) appearing in the equations which govern the behavior of the model.

Simons and Hildebrand (3) discovered in 1924 that their vapor densities could be accounted for, within the rather broad limits of experimental error, with the simple assumption of only monomer and hexamer in equilibrium: $6HF \rightleftarrows (HF)_6$. They were also able to correlate the earlier results of Thorpe and Hambly (2) with this model. Later studies (7,8) confirmed that the monomer-hexamer model provided an adequate account of association factors greater than about 1.3, but in more dilute vapor the densities

appear (5-7) to require the inclusion of polymers lower than hexamer, notably $(HF)_2$. Nevertheless, considerable evidence (*e. g.*, 12,13) has appeared in support of their ideas since Simons and Hildebrand first suggested that a hexamer might exist as the principal associated species and added the conjecture that this hexamer might be cyclic.

Among the sources of evidence which has seemed to be at odds with the dominant-hexamer view is the low-pressure vapor density study by Strohmeier and Briegleb (9), whose meticulous experimental work provided the most precise density data available for temperatures from 26 to 56 °C and pressures such that $x_\rho < 1.9$. These data overlap, without serious disagreement in general form, earlier results obtained by other workers (2-4,7); we are following Smith (13) and Maclean, Rossotti, and Rossotti (23) in choosing the data of Ref. 9 for further quantitative consideration.

Briegleb and Strohmeier were led by an analysis (22) of their own density data to conclude that preferential cyclic hexamer formation was not indicated. There are, however, grounds for disputing the validity of their analysis. To fit the experimental results, Strohmeier and Briegleb adopted (22) a model including polymers of all possible sizes, with eight independent formation constants K_j for j = 2 through j = 9, plus a ninth constant β for the ratio $K_{j\geq 10}/K_{j-1}$. That is, they fitted each density isotherm with the series

$$\sum jP_j = P_1 + \sum_{j=2}^{8} jK_jP_1^j + \sum_{j=9}^{\infty} \beta j \; {}^{j-9}K_9P_1^j, \tag{8}$$

written in closed form as

$$\sum jP_j = P_1 + \sum_{j=2}^{8} jK_jP_1^j + K_9P_1^9(9 - 8\beta P_1)(1 - \beta P_1)^{-2}. \qquad (8')$$

Ideal gas behavior was assumed and P_1 was taken as the real root[2] between 0 and $1/\beta$ of the total pressure equation

$$p = P_1 + \sum_{j=2}^{8} K_jP_1^j + \sum_{j=9}^{\infty} \beta^{j-9}K_9P_1^j \qquad (9)$$

$$= P_1 + \sum_{j=2}^{8} K_jP_1^j + K_9P_1^9/(1 - \beta P_1). \qquad (9')$$

Maclean, Rossotti, and Rossotti correctly assert (23, p. 1554) that the use of nine adjustable constants to fit each Strohmeier-Briegleb density isotherm is unwarranted. It indeed seems very unlikely that the nine parameters could be optimized to best fit the data according to a least squares criterion without some of the K_j values turning negative. Aside from this, the results of the original analysis (22) have proved unworkable on at least two additional points. If the Briegleb-Strohmeier description is used to predict association factors at saturation, the dashed curve of Fig. 2 is obtained. Clearly this curve is not in reasonable agreement with experiment, and is worst within the temperature range 26 to 56 °C where the data from which it was derived were taken. Secondly, Franck and Meyer (18, p. 850) used the constants of Ref. 22 to compute the heat capacity at 26 °C and 500 torr and obtained a result which was larger by 80%

---

[2]According to Eq. 2 of Jarry and Davis (8), p_s is slightly greater at every temperature than $1/\beta$ (22, Eqs. 7). In computations for the nearly-saturated pressure region between $1/\beta$ and p_s, therefore, care must be taken to utilize the smaller of two real roots existing between 0 and p_s.

than the experimental value.

Smith (13) suggested that the low-pressure density data can be fitted satisfactorily using a monomer-tetramer-hexamer model in which the appreciable K_2 found by Briegleb and Strohmeier (22, Fig. 5) is reinterpreted as a nonideality parameter for the monomer-oligomer mixture. He also noted that tetramer exists in amounts perhaps too small, under most conditions, to be detectable except by spectroscopic means. The suggestion that nonideal gas behavior be allowed for is well taken, but Smith's formulation, with the constants given in his Appendix II, suffers from difficulties similar to those described in the preceding paragraph, the worst being that it severely overestimates association factors when extrapolated to pressures near p_s. (Below -15.35 °C, there is also a region of pressure near p_s in which Smith's total pressure equation has no real root, but it is admittedly unfair to expect that the van't Hoff equation given by Briegleb and Strohmeier for K_2 should realistically represent the nonideality at any temperature below 26 °C.)

Maclean, Rossotti, and Rossotti (23) used graphical methods (25) to fit the Strohmeier-Briegleb density data with various models and found that a monomer-dimer-hexamer model, as well as more complicated ones, gave an acceptable fit. Of possible two-oligomer models $a_1HF + a_2(HF)_2 + a_J(HF)_J$, best results were obtained with $J = 6$. Once the data were fitted with the monomer-dimer-hexamer model, the inclusion of terms corresponding to other species could give, not surprisingly, no conclusive additional information. Extension of the results to higher pressures and lower temperatures was not attempted.

To provide a basis for direct comparison of the merits of several simple models, parameters were optimized by fitting the Strohmeier-Briegleb density isotherms using straightforward Gauss-Newton iterative minimization of the standard relative errors

$$\sigma_T = \{(n - \nu)^{-1} \sum_{k=1}^{n} [(\rho_{calc}/\rho_{obs}) - 1]^2\}^{\frac{1}{2}}, \tag{10}$$

where ν is the number of adjustable constants in the model being considered, n is the number of experimental data points defining the isotherm at temperature T, and

$$\rho_{calc}/\rho_{obs} = (\sum jP_j)/px_\rho. \tag{11}$$

These least squares calculations were done using a digital computer which was capable of improving slightly on the results obtained graphically by Maclean, *et al.*: Descriptions IV and V in Table 1 are for the same model and may be compared directly. Each isotherm was fitted individually; thermodynamic constants (Table 3) were subsequently obtained by fitting van't Hoff straight lines to the independent results from the five temperatures.

Qualitative effects of gas nonideality were apparent in calculations which incorporated a very crude allowance for departure from ideal gas behavior. Nonideality of the monomer-polymer mixture was expressed in terms of one parameter in a scheme based on the prescription outlined by Armitage, Gray, and Wright (21, p. 1803) for a mixture of HF and $(HF)_6$. Their suggestion uses the second-order virial equation for a gaseous binary mixture given by Guggenheim (26, Eq. 8.07.1):

$$\frac{v}{a_1 + a_6} = \frac{RT}{p} + \frac{a_1^2 B_{11} + 2a_1 a_6 B_{16} + a_6^2 B_{66}}{(a_1 + a_6)^2}, \tag{12}$$

which reduces to

$$p = (1 + pxB_{11}/RT)(P_1 + P_6) \tag{12'}$$

when the simplifying assumptions are made that

$$B_{66} = 6B_{11} \quad \text{and} \quad B_{16} = \tfrac{1}{2}(B_{11} + B_{66}) = (7/2)B_{11}. \tag{13}$$

The necessity for these assumptions is as stated by Armitage, *et al.* (21, p. 1803). With the same assumptions, the equilibrium condition using Guggenheim's fugacity expressions (26, Eqs. 8.08.8 and 8.08.9) becomes

$$P_6 = K_6(FP_1)^6/F, \tag{14}$$

where F is defined as $1 + pxB_{11}/RT$. The working equations for the nonideal $a_1HF + a_6(HF)_6$ model are therefore

$$p = FP_1 + K_6(FP_1)^6, \tag{15}$$

$$F = 1 + (B_{11}/RT)[p + 5K_6(FP_1)^6], \tag{16}$$

and

$$\sum jP_j = [p + 5K_6(FP_1)^6]/F. \tag{17}$$

The product FP_1 is obtained from Eq. 15 as the real positive root. Equations 12'-17 were naïvely extended by analogy to cover the ternary mixture of dimer with monomer and hexamer:

$$p = FP_1 + K_2(FP_1)^2 + K_6(FP_1)^6 \tag{15'}$$

$$F = 1 + (B_{11}/RT)[p + K_2(FP_1)^2 + 5K_6(FP_1)^6] \tag{16'}$$

$$\sum jP_j = [p + K_2(FP_1)^2 + 5K_6(FP_1)^6]/F \tag{17'}$$

The derivatives of the difference $\delta = [(\sum jP_j)/px_\rho - 1]$ needed for the least squares calculation are

$$\partial\delta/\partial K_j = (FP_1)^j(j - 1 - c)/px_\rho F^2 \qquad j = 2,6 \tag{18}$$

and

$$\partial\delta/\partial(B_{11}/RT) = -(\sum jP_j)^2/px_\rho. \tag{19}$$

The symbol c in Eq. 18 is defined by

$$c = [2K_2(FP_1)^2 + 30K_6(FP_1)^6]/(F\sum jP_j). \quad (20)$$

Results from least squares calculations for a few simple models are summarized in Tables 1-3; descriptions by other authors, and their standard errors of fit, are listed for comparison. There is no clear justification for preferring the Briegleb-Strohmeier formulation, Descriptions I and II, especially at the three upper temperatures. A model (VIII) analogous to Smith's (III), but with dimer considered instead of nonideality, could not be optimized without getting negative values for K_4. Unreasonably large values were obtained for $-B_{11}/RT$, and hence for association factors at saturation, if this nonideality parameter was varied in the least squares process. Description IX is an example. For Description VII, therefore, B_{11} was held fixed at the Berthelot gas value (27, p. 187, Eq. 16-15). The adjustable parameters in Models V-VII, then, were K_2 and K_6. Description V is simply a refinement of IV, as mentioned earlier. Description VI is for the model of Franck and Meyer (18) optimized to fit the density data; these results differ insignificantly from the pure ideal monomer-dimer-hexamer Description V. Additional comments on the Franck-Meyer model appear in the next subsection.

Association factors at saturation based on Descriptions V and VII are plotted in Fig. 2. Both curves are much more reasonable throughout the range -80 to +60 °C than is the dashed curve for Description II by Briegleb and Strohmeier. At temperatures above 60 °C the ideal monomer-dimer-hexamer model cannot be expected to give accurate association factors near $p = p_s$ because the vapor pressure becomes quite large and effects of nonideal-

Table 1. Standard deviations σ_T, in percent, measuring quality of fit to Strohmeier-Briegleb density data by various models

Description		I	II	III	IV	V	VI	VII	VIII	IX
Source		a	b	c	d	e	e	e	e	e
Model		j=1,...,∞ ideal	j=1,...,∞ ideal	j=1,4,6 nonideal	j=1,2,6 ideal	j=1,2,6 ideal	j=1,...,∞ ideal	j=1,2,6 nonideal	j=1,2,4,6 ideal	j=1,6 nonideal
ν		9	9[f]	3	2	2	2	2[g]	3	2
Temp.	n									
26 °C	33	.36	.52	.47	1.77	.99	1.00	.78	h	.25
32	25	.58	.60	.45	1.65	.92	.93	.71	h	.24
38	22	.39	.44	.28	.52	.43	.45	.35	h	.16
44	18	.13	.19	.22	.13	.088	.093	.082	h	.077
56	15	.14	.16	.16	.21	.075	.074	.073	.077	.077

[a] Briegleb and Strohmeier (22, Tabelle 1).

[b] Briegleb and Strohmeier (22, Eqs. 7).

[c] Smith (13, Appendix II).

[d] Maclean, Rossotti, and Rossotti (23, Table 1).

[e] Constants were derived in the present work by least squares; see Table 2.

[f] Use of $\nu = 9$ was for convenience in computing σ_T; actually only 18 constants covered all five temperatures.

[g] B_{11} was held fixed at the Berthelot gas value; K_2 and K_6 were varied.

[h] Results were rejected because calculations gave $K_4 < 0$.

Table 2. Equilibrium constants, nonideality parameters, and association factors for saturated conditions. For "(-m)" read "(10^{-m})." Square brackets denote values which are unacceptable.

Temp.	Descr.	$-B_{11}/RT$	B[a]	K_2	K_4	K_6	$x_\rho[p_s(T)]$
26 °C			1.55(-4)		2.17(-10)	4.83(-15)	
32			1.21(-4)		1.03(-10)	1.25(-15)	
38	III		.95(-4)		5.36(-11)	3.40(-16)	
44			.74(-4)		2.84(-11)	9.63(-17)	
56			.46(-4)		8.63(-12)	9.10(-18)	
26				1.58(-4)		1.15(-14)	
32				1.20(-4)		3.16(-15)	
38	IV			1.00(-4)		8.91(-16)	
44				8.71(-5)		2.40(-16)	
56				5.75(-5)		2.34(-17)	
26				1.25(-4)		1.31(-14)	2.961[b]
32				9.24(-5)		3.56(-15)	2.814[b]
38	V			9.44(-5)		9.27(-16)	2.675[b]
44				8.23(-5)		2.50(-16)	2.539[b]
56				5.12(-5)		2.52(-17)	2.293[b]
26				1.16(-4)		1.30(-14)	
32				8.59(-5)		3.52(-15)	
38	VI			8.90(-5)		9.13(-16)	
44				7.84(-5)		2.42(-16)	
56				4.97(-5)		2.27(-17)	
26		2.95(-5)[c]		1.02(-4)		1.15(-14)	3.191[b]
32		2.77(-5)[c]		7.21(-5)		3.06(-15)	3.058[b]
38	VII	2.61(-5)[c]		6.94(-5)		7.92(-16)	2.929[b]
44		2.45(-5)[c]		5.61(-5)		2.12(-16)	2.806[b]
56		2.18(-5)[c]		2.80(-5)		1.99(-17)	2.580[b]
26				--	[<0]	--	
32				--	[<0]	--	
38	VIII			--	[<0]	--	
44				--	[<0]	--	
56				5.02(-5)	3.52(-12)	2.08(-17)	
26		[1.71(-4)]				6.21(-15)	[5.077]
32		[1.32(-4)]				1.76(-15)	[4.542]
38	IX	[1.05(-4)]				5.01(-16)	[4.140]
44		[8.09(-5)]				1.51(-16)	[3.723]
56		[4.96(-5)]				1.59(-17)	[3.143]

[a] B = nonideality parameter in Smith's model = K_{12} of Ref. 22.

[b] Smoothed values of Fig. 2.

[c] Berthelot value, not varied.

Table 3. Comparison of thermodynamic parameters

Description	II	III	IV	V	VII		
Source of constants	a	b	c	d	d'	e	f
$-\Delta H_{1,2}$, kcal/mole	7.9		6.4±0.9[g]	5.3±2.7	7.9±3.4	6.7	
$-\Delta S_{1,2}$, eu	43.8		38.8±3.0	36±9	45±11	39	83.20
$-5\Delta S_{1,2}$	219.0			178	223	195	
$-\Delta H_{i,i+1}$, kcal/mole	5.8-8.2					6.7	
$-\Delta S_{i,i+1}$, eu	32.7-42.3					39	12.80
$-5\Delta S_{i,i+1}$	163.5-211.5					195	
$-\Delta H_{1,6}$, kcal/mole	40.0	40	40.6±0.9	41.1±1.1	41.7±0.8	40.2	
$(-\Delta H_{1,6})/6$	6.67	6.7	6.76	6.85	6.94	6.70	
$-\Delta S_{1,6}$, eu	200.5	199	199.3±3.0	200.6±3.5	203.0±2.6	199	

[a]Briegleb and Strohmeier (22, Tabelle 2).

[b]Smith (13).

[c]Maclean, Rossotti, and Rossotti (23, rederived from Table 1).

[d]This work.

[e]Franck and Meyer (18, Tabelle 5).

[f]Hu, White, and Johnston (14, Eqs. 11,12).

[g]Uncertainties (99.73% confidence) were reckoned from scatter in log K *vs.* T^{-1} plots.

ity cannot be neglected. At very low temperatures (below -30 °C) the theoretical curves may be slightly too high, reflecting a small difference between vapor pressures given by Eq. 1 of Jarry and Davis (8) and observed pressures (28). Possible errors in the circled experimental points and the significance of the point located by the cross in Fig. 2 are discussed under "Thermal properties." The need for better experimental data on large x_ρ values is apparent in Fig. 2. It would be particularly interesting to examine accurately the saturated vapor below -50 °C to see whether or not x_ρ values larger than 5 can actually occur.

In view of the crude approximations made in treating nonideality, only limited quantitative significance can be attached to the results of Description VII. It is enough to point out that association factors at saturation are quite sensitive to the effect of nonideality, while the hexamer thermodynamic parameters are not and the dimer ΔH and ΔS are moderately sensitive, but are subject to rather large uncertainties. The dimer mole fraction implied by the nonideal gas Description VII is always less than that computed from Description V, the ideal monomer-dimer-hexamer mixture. Accordingly, taking Description V as giving generous estimates of dimer mole fraction, it is found that dimer never exceeds 6.5 mole percent in saturated vapor below 56 °C. Furthermore, the largest dimer contribution to an electron diffraction f(r) peak will not exceed 3.5% at 24 °C and below, provided that the association factor is at least 2.0 and the hexamer is cyclic.

In summary, careful consideration of the available vapor density data has led to the conclusion that although minor improvements in representa-

Fig. 2. Association factors for saturated conditions.
Experimental points denoted by squares, triangles, and circles are from Refs. 3, 4, and 8, respectively. The curves represent values predicted according to Descriptions II, V, and VII as specified in the text and Tables 1-3. Values of p_s were reckoned using Eq. 1 of Ref. 8. The point marked by the cross is discussed on pp. 22-23.

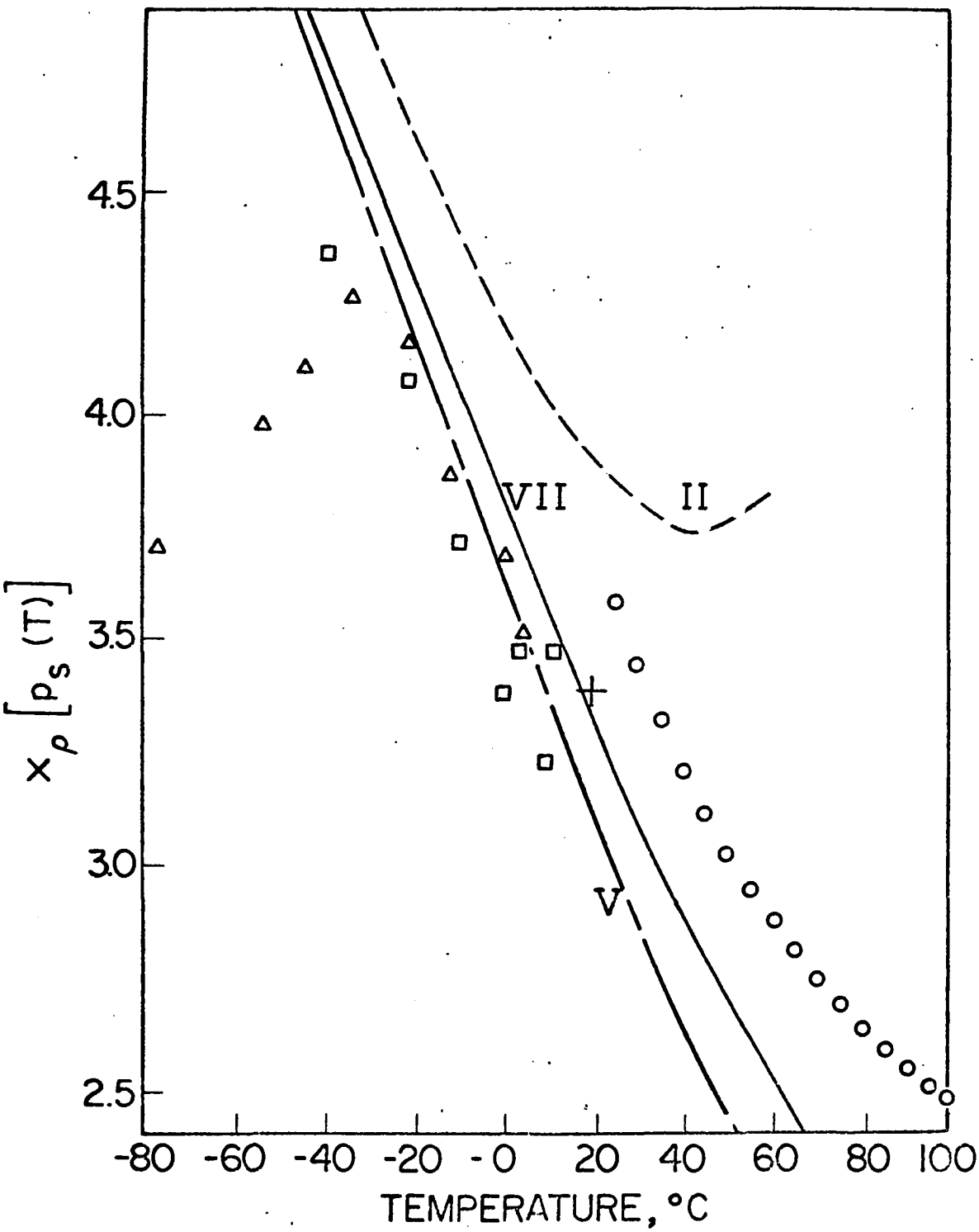
4.5
4.0
3.5
3.0
2.5
$X_\rho [\rho_s(T)]$
VII
II
V
-80 -60 -40 -20 -0 20 40 60 80 100
TEMPERATURE, °C

tion of the data might attend use of more complicated models, no necessity to consider appreciable amounts of species other than HF, $(HF)_2$, and $(HF)_6$ at temperatures not above 56 °C has been substantiated in prior density studies. In what is believed to be the first attempted demonstration that one model can be employed at all pressures up to p_s and all temperatures up to at least 56 °C, it has been shown that a scheme involving only monomer, dimer, and hexamer gives the most satisfactory account to date of observed vapor densities throughout this p-T region. The existence of other species such as $(HF)_{3-5}$ is possible, but amounts large enough to contribute appreciably to macroscopic properties such as vapor density have not so far seemed necessary.

3. Thermal properties

Franck and co-workers collected data on the thermal conductivity (19) and heat capacity (16-18) of associated HF vapor. The results were accounted for by a model in which the cyclic hexamer is favored, but which also includes a distribution of chain species in minor amounts. The assumed system of equilibria among chain polymers is essentially the Briegleb-Strohmeier model simplified by assuming the same equilibrium constant for each monomeric addition step. That is (for chains only),

$$P_j/P_1^j = K_j = K_2^{j-1}. \qquad (21)$$

In addition to noting that heat capacities computed from the Briegleb-Strohmeier array of constants could be in error by 80%, Franck and Meyer further showed (18, p. 579) that the simplified chain-only model could not be made to fit the heat capacities observed at 26 °C; this conclusion presumably holds for lower temperatures and for at least some moderate range

above 26 °C as well.

The cyclic hexamer invoked to account for the thermal data was thought to derive its special stability from the possibility of ring formation from six-membered chains at a very small cost in entropy of ring closure. (Compare $\Delta S_{1,6}$ with $5\Delta S_{1,2}$ or $5\Delta S_{i,i+1}$ in Table 3.) The relative dominance of the 6-ring then diminishes with increasing temperature.

The model of Franck and Meyer appears to have merit beyond its ability to account for thermal data. In the temperature region below 26 °C, which is of interest in the present electron diffraction study, the model reduces to a monomer-dimer-hexamer mixture, with dimer a minor contributor and other acyclic chains completely negligible. It has already been shown that such a three-species scheme is capable of fitting the high-precision vapor densities quite well, with thermodynamic parameters derived from such a fit differing insignificantly from those found by Franck and Meyer (18, Tabelle 5).

It is noteworthy here that the average entropy of association (16.0 eu in saturated vapor at 292.61 °K) computed by Franck and Meyer is in good agreement with the experimental value 17.53 eu obtained by Hu, White, and Johnston (14). This is in contrast with a much less satisfactory value (26.93 eu) computed by the latter investigators using a pure monomer-hexamer model. It must also be noted that in their association entropy calculation (result 20.2 eu) purporting to show preference for a chain-distribution model, Hu, *et al.* relied on ΔS values (last column of Table 3) which are not comparable with values found by any other workers. It is therefore concluded that the Franck-Meyer model does not conflict with the

experimental results of Ref. 14.

Hyman and Katz (29, pp. 53-54) have called attention to the discrepancy between the heat of vaporization obtained calorimetrically by Hu, White, and Johnston (14) and results derived from vapor pressure data by Jarry and Davis (8), who were themselves aware that Fredenhagen's earlier values (4) were considerably larger than their own. There is also an appreciable discontinuity (8, Fig. 3) between association factors measured by Jarry and Davis for saturated vapor above the normal boiling point and those previously determined at lower temperatures by others. Because the vapor density enters the Clapeyron equation used to find ΔH_{vap} from the vapor pressure curve, therefore, it seems possible that the source of the discrepancy is an error in the density measurements of Ref. 8, perhaps due to the presence of excess HF as a condensed phase in the vapor sampling vessel. The very description (8, p. 601) of the experimental procedure explicitly suggests that liquid HF "spray" was present in the vapor container prior to isolation and weighing; no mention is made of any attempt to detect incomplete drainage of liquid from the vessel in the allotted five minutes.[3] Serious (>10%) errors in the measured densities would have resulted from as little as 0.5 mg/cm^2 coating the interior surface of the vapor container, and any such persistent excess would have been subsequently pumped into the weighing vessel along with the actual vapor of interest.

In any case, the heat of vaporization at 292.61 °K found by applying

---

[3]Strohmeier and Briegleb (9, p. 665) took elaborate precautions to assess this sort of error in their low-pressure experiments.

the Clapeyron equation to the empirical vapor pressure Eq. 2 of Jarry and Davis is brought into excellent agreement with the calorimetric value 1789.89 cal/20.01 g if the association factor 3.763 used originally is replaced by the value 3.342 taken from the solid curve of Fig. 2: The corrected result is 1806 cal/20.01 g, while the original calculation gave 1608. The x_ρ value needed to give essentially exact agreement is 3.380; this point is marked by a cross in Fig. 2.

4. Infrared absorption intensities

D. F. Smith has been given due credit (29, pp. 55,59; 12, p. 15) for his very lucid work (13,24) on the infrared spectra of HF and DF polymers. It is now a simple matter to point out that his conclusions are in accord with the model of Franck and Meyer: He found a predominating hexamer, along with dimer in smaller amounts and a tetramer in quantities likely to contribute little to the nonspectroscopic properties of the vapor.

5. Dielectric polarization

Dielectric polarization measurements by Magnuson (12) have furnished strong evidence for the cyclic nature of whatever polymers predominate. These results do not agree with the earlier work of Oriani and Smyth (11), but were obtained with allowance for departure from ideal gas behavior and with precaution against spurious effects due to HF adsorbed on the walls of the experimental vessel, and therefore seem to be definitive.

6. Other evidence

X-ray diffraction (30) has shown that crystalline HF consists of infinite planar zigzag chains. From this it might be argued that oligomeric

chains, of various lengths, are to be expected in the vapor. It seems equally reasonable to expect, however, that if HF indeed prefers to form endless chains, it would do so in the vapor by cyclization.

The previous electron diffraction study (10) of gaseous HF polymers showed, by detecting several diffraction rings corresponding to an internuclear distance of ∿2.5 Å, that some sort of hydrogen-bonded aggregate persisted long enough after exiting the sample nozzle to be detectable in a diffraction experiment. Not enough data of sufficient accuracy were available, however, to firmly establish the additional structural conclusions which were drawn. The value 140 ± 5° reported for the mean FFF angle in the polymers, particularly, is compatible with neither a hexagonal structure nor, as will be shown, with the new electron diffraction results obtained in this laboratory.

A search (31) of the ultraviolet wavelength range down to 1500 Å disclosed a featureless temperature-dependent absorption between 54,000 and 67,000 cm^{-1}. The fact that no discreet bands were found was interpreted as "a good reason to think that there are no, or very few, cyclic F_6H_6 molecules in the associated vapor," but no further justification for this conclusion was given.

Nuclear magnetic resonance data (32) were recently surmised to be not incompatible with the existence of a lone cyclic six-membered polymer in the vapor.

There seem to have been no fruitful attempts to interpret quantitatively the free-polymer infrared absorption frequencies or to study the gaseous oligomers by Raman, microwave, or mass spectroscopy.

7. Summary

It now seems that all of the reliable physical evidence considered here is in accord with the following essential points. The principal constituents of HF vapor are monomer, dimer, and hexamer, and the amount of dimer is limited. The hexamer is very probably cyclic. The existence of other oligomers is likely, but in concentrations which are, for most nonspectroscopic experimental purposes, negligible by comparison with the monomer-dimer-hexamer total.

Experimental Procedure

Electron diffraction experiments for this study were conducted with intent to obtain structural data for gaseous hydrogen fluoride in as highly polymerized a form as was feasible. Accordingly, diffraction patterns were recorded using relatively large sample pressures to favor a high degree of association in the specimen beam. Data on the temperature dependence of the diffraction pattern were also collected to furnish clues to whatever changes might occur with changing association factor.

In the problem at hand, the conventional index of resolution R which measures experimental efficiency is not separable from structural (distance multiplicity) and concentration unknowns which have to be determined from the experimental data. Therefore R was initially fixed at the ideal value 1.0 as a working assumption. Attention was then given in the experimental work and data analysis, however, to possible pressure-related and other effects capable of influencing R and thence the structural conclusions derived.

1. Apparatus and materials

Two series of electron diffraction photographs of HF vapor were made using an apparatus described elsewhere (33,34). In order that the specimen beam have as large a proportion of the heavier polymeric species as possible, a valved sample reservoir containing liquid HF was connected directly to the inlet line; the effective sample pressure upstream from the nozzle was therefore as near to the saturation vapor pressure as could conveniently be arranged. During the first series of experiments the sample container and injection line were at the ambient laboratory temperature, approximately 22 °C. For the second series, inlet tubing and sample reservoir were enclosed in a jacket through which a coolant (dried air chilled in a dry-ice slush) could be circulated. With this arrangement the sample cell and the upstream end of the injection line were held at approximately -19 °C, while the nozzle end of the line was at about -37 °C. The temperature gradient was mostly due to thermal contact between the cooling jacket and the vacuum wall of the diffraction chamber, and could not be easily avoided. The effect of a temperature decrease in the direction of sample flow was advantageous in these experiments, however, because it would tend to counter the dissociative effect of the inevitable pressure drop in the same direction.

Anhydrous liquid hydrogen fluoride was supplied in lecture bottles by The Matheson Company, Inc. Purity of the liquid phase was specified by the manufacturer to be at least 99.9 mole-percent. The material was used without further purification, except whatever may have incidentally attended filling of the sample cells by vacuum distillation at 0 °C.

The sample system used for the room-temperature experiments was made entirely of Kel-F (35, p. 60), excepting the nozzle tip, which was platinum. The jacketed low-temperature injection system had Teflon gaskets at all joints and a nozzle tip of nickel, but was otherwise of Monel metal. The transfer line through which the sample cells were filled consisted of nickel tubing silver-soldered to Monel metal Hoke bellows valves which were fitted with Teflon gaskets.

2. Recording diffraction patterns

Data in the interval $3.2 < s < 40.5$ Å^{-1} were obtained from photographs made at nozzle-to-plate distances nominally 21 cm (long distance) and 11 cm (medium distance) with the usual radius-cubed rotating sector (33,36). Corrections for imperfections in the shape of this sector were made according to the argon-based calibration previously in routine use in this laboratory. Additional data for $2.1 < s < 14.9$ were taken at the long distance using a radius-squared (quadratic) sector of 34 mm maximum radius. This sector was calibrated with neon, which is isoelectronic with HF, and the calibration curve agreed well with the results of an optical calibration done earlier (37). Background functions for the leveled quadratic-sector data were quite smooth, though not horizontal, throughout the s range from $\sim$2.1 to $\sim$15; specifically, these backgrounds were free of the troublesome bends sometimes encountered (36,38) in the vicinity of $s = 6$ or 7.

Diffraction patterns were recorded on 4 × 5 in. Kodak Process Plates. An approximate correction (39) to remove the "edge effect" (40) which these plates exhibit (41) was applied through division of observed optical densities measured at distances y more than 24 mm from the center of a plate

by $[1 + 0.000125(y - 24)^2]$. All densities were then converted to values of exposure E according to the emulsion calibration equation[4]

$$E = D + 0.05D^3. \tag{22}$$

Additional information concerning experimental conditions appears in Table 4.

3. Extraneous intensities

During at least one typical experimental run with each configuration of the apparatus, a blank exposure was made in the absence of specimen flow to record extraneous intensities. Residual gas pressure during a blank exposure was always between 10^{-5} and 4×10^{-5} torr. The extraneous intensity corrections indicated by ordinary blanks of the sort just described are in general reduced to trivial levels whenever very short exposure times are appropriate for the sample under study, and the blank plate intensities obtained here usually amounted to only about 0.2% of the total HF diffraction pattern intensities; the largest value observed was approximately 0.5%. In contrast, blank intensities as a percentage of the neon calibration pattern intensities were an order of magnitude larger (2-5%). That is, they were comparable with values observed elsewhere in work with light noncondensible gases at low inlet pressures (40, Table V, 29 cm N_2 and O_2 data).

Even though sample pressures greater than 1 atm were used, the diffraction unit's fast diffusion pumping system, aided by a large liquid nitrogen-cooled condensing surface 10 cm from the nozzle, was able to keep

---

[4]See pp. 92-100.

Table 4. Experimental conditions for HF diffraction photographs

Approx temp., °C	+22			-19		
Approx vapor pressure,[a] torr	830			163		
Electron wavelength, Å	.06015			.06015		
Nozzle orifice diam, mm	.20±.03			.28±.03		
Beam current, μA	.364			.385		
Plates taken at	Iowa State University			University of Michigan		
Date	1965			1966		
Sector	quadratic	cubic	cubic	quadratic	cubic	cubic
Nozzle-to-plate distance, mm	210.50	210.54	108.81	209.15	209.23	106.99
Exposure time, sec	.1	.8-1.0	2	.5	5	12
Number of plates averaged	7	5	5	4	4	4
Blank intensity, percent of total	.22-.33	.18-.21	.19-.28	.23-.52	.14-.30	b
Percent of blank intensity subtracted	100	100	0	100	100	0
σ(D),[c] percent	.2 - .3	.11-.18	.09-.28	.045-.072	.045-.060	.029-.031[d]
σ(I),[e] percent	.19-2.9	.47-3.3	.22-.92	.099-.152	.146-.370	.069-.188

[a] Jarry and Davis (8, Eq. 1).

[b] Blank was too light for accurate microphotometry.

[c] See p. 31.

[d] For one plate σ(D) was 0.274, due to readings being taken at slightly unequal distances from the center of the pattern.

[e] See p. 32.

the background pressure below 10^{-3} torr, as indicated by a hot-cathode ionization gauge which was monitored during sample injection. Still it may be supposed that the blanks described above underestimate the true extraneous intensities effective during an actual diffraction exposure, because the contribution of scattering by delocalized specimen gas was absent. This contribution, for example, appears (40) to add approximately 30-50% to the applicable blank intensities in the case of gases like N_2 and O_2. An experimental attempt to assess the scattering to be expected in the present work from delocalized HF was made by a method similar to one outlined elsewhere (33, Footnote 7): A plate was exposed under the same conditions used for the long-distance, quadratic-sectored HF plates taken at -19 °C, except the electron beam was aligned to pass about 2 mm to the side of and slightly behind the exit end of the nozzle. This plate had a faint pattern similar in shape to the analogous exposure patterns taken with the electron beam directly intersecting the stream from the nozzle, but it was less than 3% as strong (*i. e.*, 5-8 times the ordinary blank intensity). From these observations it seems reasonable to conclude that neglect of corrections for delocalized extraneous scattering in this study would result (42) in a diminution of not more than 3-4% in the indices of resolution. Data obtained in the delocalized-scattering experiment also indicate that extraneous scattering contributes appreciably to the upsweep of backgrounds at larger scattering angles.[5]

---

[5] *Cf.* Fig. 3 and Refs. 36, 43, and 44. Recall that a correction for the edge effect was applied in the present study.

4. Reproducibility

Two statistical measures of the reproducibility of the electron diffraction intensity measurements appear in Table 4. The reproducibility of a microdensitometric exposure determination made at a particular plate radius, based only on the distribution of differences between readings taken on the right and left sides of center as a single spinning plate is scanned by the microphotometer, is measured by $\sigma(D)$:

$$2\sigma_k(D) = 100\{J^{-1}\sum_{j=1}^{J}[(E_{right} - E_{left})/E_k]^2\}^{\frac{1}{2}}, \qquad (23)$$

where k is the index of one plate in a set of K plates, plate k is read at J points on each side, and $E_k = \frac{1}{2}(E_{right} + E_{left})$ for each $j = 1,\ldots,J$. Included in $\sigma(D)$ are effects of microphotometer circuit noise and whatever contribution accrues from reading E_{right} and E_{left} at slightly different distances from the true center of the diffraction pattern. Values of $\sigma(D)$ between 0.01 and 0.06% are at the limit of precision attainable with the present photographic plates and densitometric equipment.[6] The fact that $\sigma(D)$ values were appreciably better, by about fivefold, for the low-temperature plates (Table 4) reflects only a change in microphotometer electronics: A new phototube current preamplifier with improved linearity, stability, and response time was installed after the room-temperature plates were read.

The quantity $\sigma(I)$ is the standard deviation measuring platewise reproducibility of the diffraction pattern shape. It is computed as the rms deviation for an individual plate from the mean intensities for an entire

---

[6]See pp. 80-88.

set.

$$\sigma_k(I) = 100\{J^{-1} \sum_{j=1}^{J} [E_k/(c_k E) - 1]^2\}^{\frac{1}{2}}, \quad (24)$$

where the mean exposure at radial point j is

$$E = K^{-1} \sum_{k=1}^{K} (E_k/c_k), \quad (25)$$

and c_k is the inverse of the weight factor for plate k:

$$c_k = J^{-1} \sum_{j=1}^{J} (E_k/E_1). \quad (26)$$

The deviation $\sigma(I)$ includes the small effect of $\sigma(D)$ noise, and contains additional contributions from plate-to-plate variations in backgrounds and in the scattering source due to pressure and temperature effects. The largest $\sigma(I)$ values for the -19 °C data compare favorably with the best results heretofore obtained with other specimen gases more likely to give reproducible scattering sources. At room temperature, $\sigma(I)$ values above 3% occurred, but were due to fluctuations in the smooth background, not to short-range noise in the molecular interference pattern. The $\sigma(I)$ values at the low ends of the ranges given for the 22 °C data are therefore considered to be more nearly representative of the noise level which is of significance for purposes of structure determination.

Reproducibility of the experiment can also be checked by observing how well the M(s) data for various s ranges match in the regions of overlap. The present HF data overlapped well; no gross discrepancies in M(s) amplitude, which would indicate inconsistent index of resolution or degree of association, were apparent.

Over-all confidence in the results from the two sets of photographs is enhanced by noting the extensive similarities, to be discussed below, in view of their persistence through not only a lowering of the temperature, but also the following: dismantling and relocation of the diffraction unit, use of samples from different manufacturer's batches, a change in container materials, alterations in the microphotometer detector circuitry, and lapse of a year's time between the sets of experiments.

5. Preliminary reduction of data

Leveled experimental intensities, reduced molecular intensities M(q), and radial distribution functions f(r) were obtained from the photographic exposure data by methods similar to those described elsewhere (45,46). The Degard damping factor used for computing experimental f(r) curves was $[\exp(-0.00125s^2)]$.

Results and Discussion

Results of the diffraction experiments are depicted in Figs. 3-5. The final experimental radial distribution functions appear in Fig. 5 as solid curves. Each f(r) curve consists of four peaks, none unambiguously resolvable into components, which will be referred to hereafter by number from left to right. The diffraction data consisting of more than 6,000 intensity measurements can be satisfactorily explained with the assumption of a single species as the principal oligomeric constituent of the scattering vapor. That species has a skeleton of fluorine atoms which is in the form of a flexible six-membered ring. After least-squares refinement of the parameters defining such a model, the rms deviation between observed and

Fig. 3. Leveled experimental total intensities and background functions for hydrogen fluoride vapor at nominal temperatures of +22 and -19 °C. Data shown were leveled and corrected for sector asperities as described in Ref. 45.

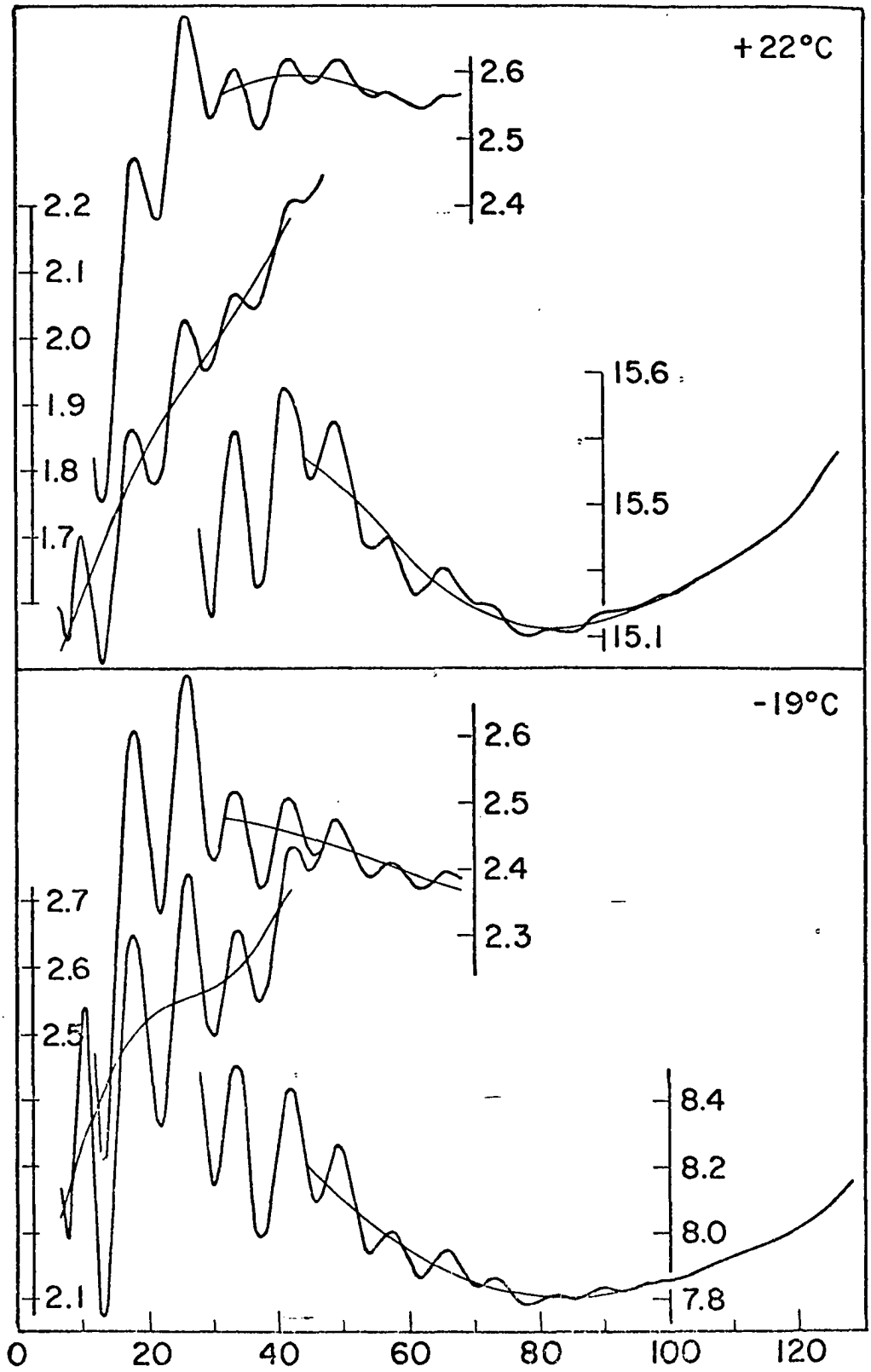
+22°C
2.6
2.5
2.4
2.2
2.1
2.0
1.9
1.8
1.7
15.6
15.5
15.1
-19°C
2.6
2.5
2.4
2.3
2.7
2.6
2.5
2.1
8.4
8.2
8.0
7.8
0
20
40
60
80
100
120

Fig. 4. Reduced molecular intensity curves qM(q) for hydrogen fluoride vapor, calculated directly from the data of Fig. 3

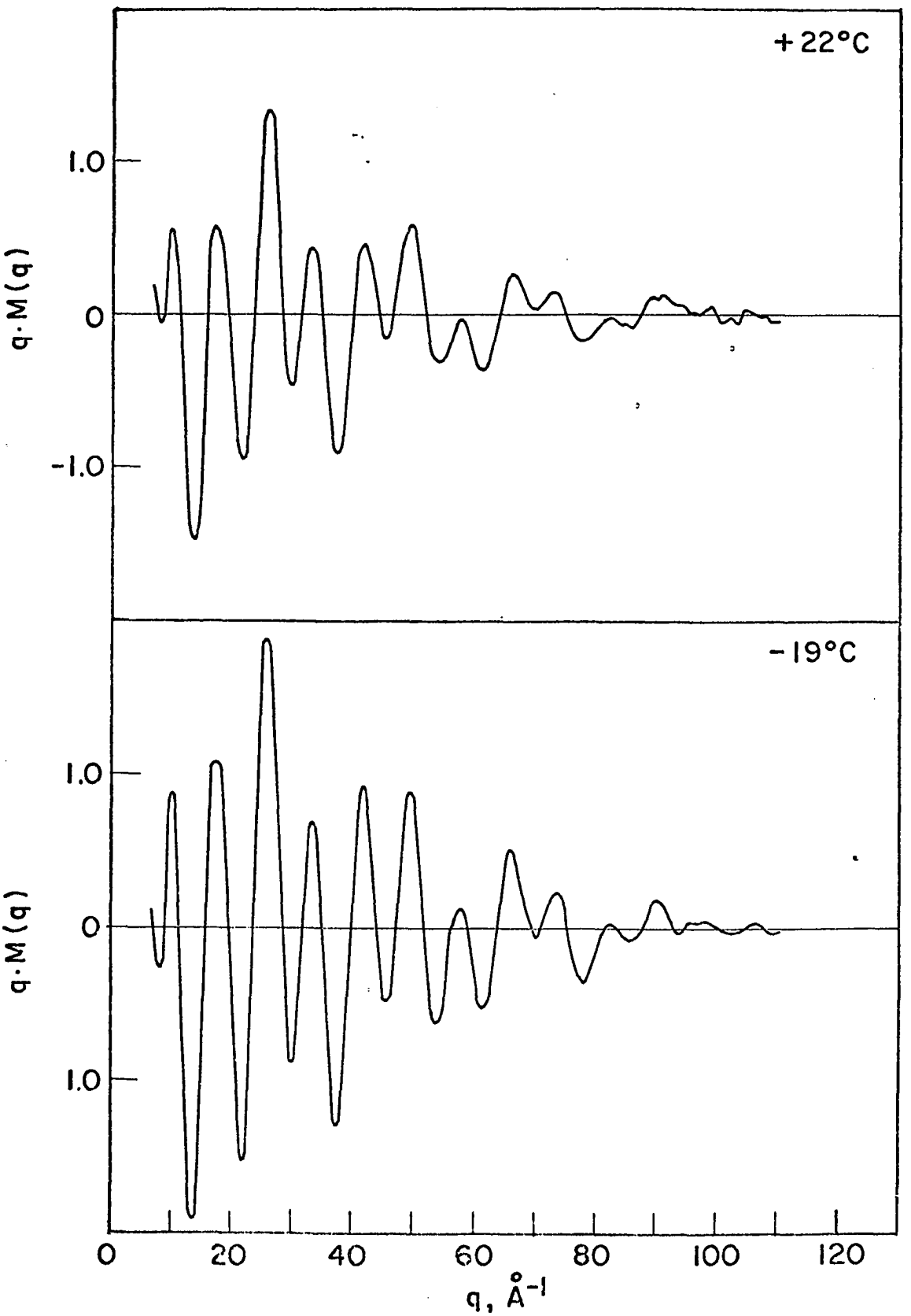
+22°C
-19°C
1.0
0
-1.0
q·M(q)
0
20
40
60
80
100
120
q, Å⁻¹

Fig. 5. Radial distribution functions.
Solid curves are from Fourier inversion of experimental data. Dashed curves represent theoretical functions calculated from the assumption that the mean position of every hydrogen-bonding proton is approximately as sketched. The $\Delta f(r)$ curves show differences between the experimental results and the $f(r)$ calculated for the best model.

DASHED CURVES:

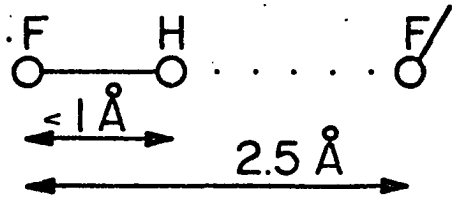

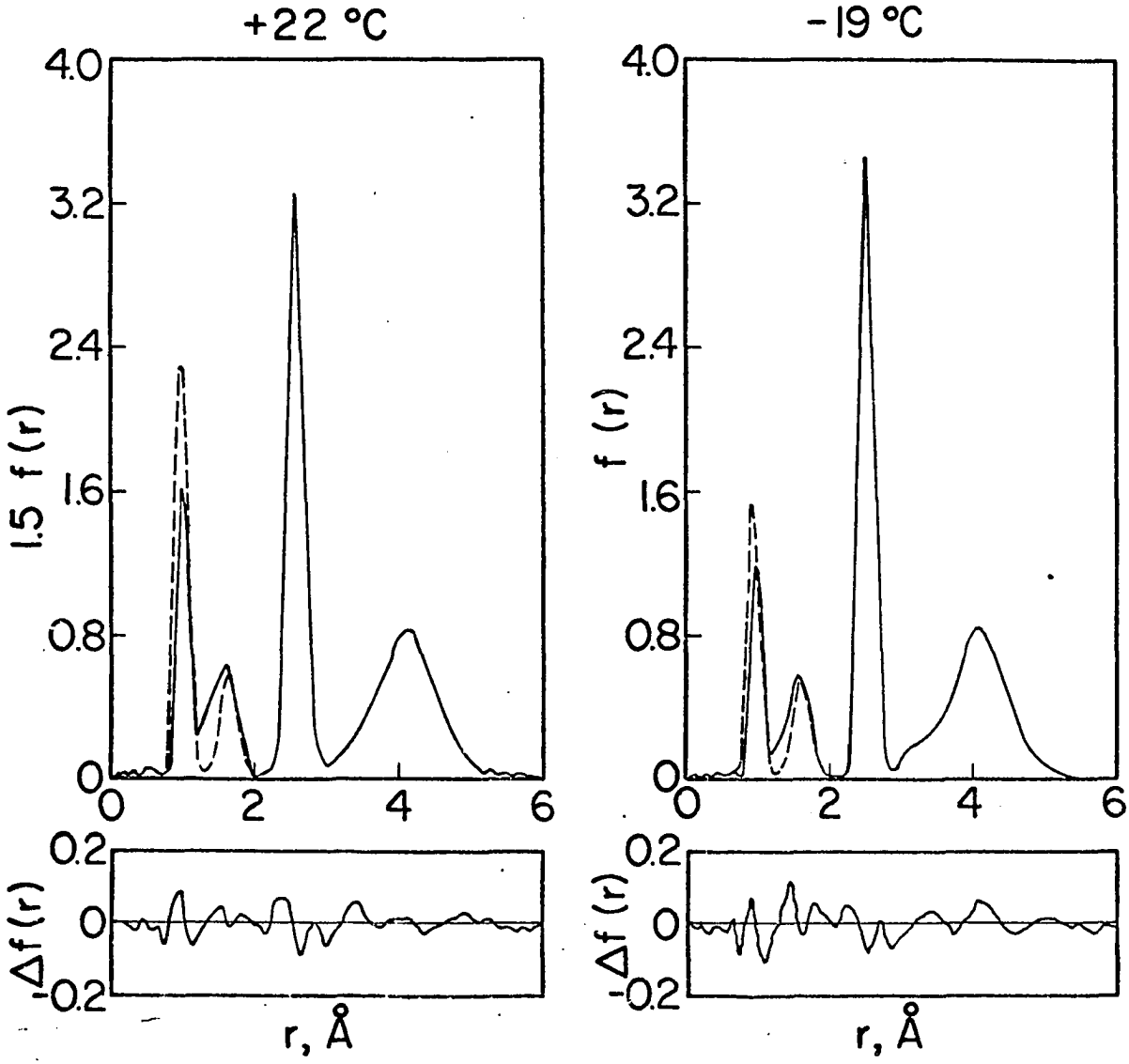

calculated intensities was of the order of 2 parts per thousand. Differences between theoretical and experimental f(r) curves are plotted at the bottom of Fig. 5 and do not exceed common levels of f(r) noise.

Before discussing further the characteristics of the favored model it will be useful to outline some of the reasoning, including unfavorable aspects of possible alternative interpretations, which led to its adoption. It should be borne in mind throughout the discussion that this type of analysis of a mixed vapor, for which neither composition nor possible structures of the components is known in advance, is more difficult and subject to greater uncertainty than conventional electron diffraction analyses.

At the outset it was assumed that association factors found by vapor density measurements on saturated vapor could be used as rough estimates of upper bounds on molecular weight averages likely to be encountered in the diffraction experiments. Within the limits of this assumption, but without geometric or mass conservation constraints, a mathematical model was used in the process of f(r) refinement until good, physically-interpretable f(r) results were obtained. The refinement proceeded at first by pure trial and error, and then by a cyclic process of adjusting the model, peak areas and all, to agree with the experimental f(r), followed by improvement of background functions under smoothness and nonnegative f(r) criteria. This process of refining f(r) continued until implications concerning gross geometry of the oligomer fluorine skeleton became clear; only then was geometric consistency corresponding to a particular model introduced and the model refined by least squares fitting of the observed intensities and

by continued visual comparison of experimental and calculated f(r) curves. Because solution of the structure depends heavily on the experimental f(r) peak areas, it is gratifying that the development of the experimental f(r) curves converged to give physically-interpretable results in the absence of area constraints such as are tacitly assumed in routine work. Indeed, the areas of experimental Peaks 1-4 appeared sufficiently insensitive to the assumed model so that their uncertainties could be roughly estimated as <8%, <10%, 5%, and 30%, respectively.

The observed areas of Peaks 3 and 4 at once suggest in a straightforward way the qualitative conclusions to be drawn concerning gross geometry of the oligomer fluorine atom skeleton. In the low-temperature instance, the area of experimental Peak 3, which represents the hydrogen-bonded FF distances, is too large, relative to the maximum number j-1 of such distances possible in an acyclic species of length j monomer units, for the data to be explained in terms of any mixture having a plausible association factor and containing only acyclic (chain-type) species. The data might be fitted with a chain-only model if the association factor were taken near 7, but that is well above the largest reasonable value (*i. e.*, ≤5 even in saturated vapor at -50 °C). On the other hand, the -19 °C data are well represented by an equimolar mixture of monomer with cyclic hexamer. The association factor of this $1HF + 1(HF)_6$ model is 3.5, a value not exceeding the saturation limit at any temperature below +5 °C; at -19 °C the limiting value is ≥4.1.

The third f(r) peak in the room-temp. instance is not large enough to show insufficiency of acyclic models by means of the same argument, but the similarities between the radial distribution functions for the two temper-

atures justify the assumption that the same sort of model should be applicable in both cases. Furthermore, the very similarity of the two polymer patterns (Peaks 2-4) is itself an important clue. The room-temp. curve of Fig. 5 is plotted on a vertical scale expanded 1.5 times so that the shapes of the two observed radial distribution functions can be readily compared. The shape of the polymer pattern changes very little on lowering the temperature by at least 41°, while the intensity of polymer features increases appreciably, as is also apparent in Fig. 4. This is the behavior to be expected of a single associated species mixed with monomer in temperature-dependent proportions. If the polymers were principally open chains whose average length increased with increasing association factor, the temperature difference of the diffraction experiments should be expected to produce some significant dissimilarity between the distributions of long non-bonded (Peak 4) distances. That Peak 4 does not appreciably shift position with temperature is clear from the data. There is also no indication that the ratio of areas of Peaks 3 and 4 is temperature dependent, although a possibility of a modest dependence remains because of the uncertainties of the fourth-peak areas. Nevertheless, an extended planar zigzag chain model could not reasonably account for more than about 40% of the Peak 4 areas displayed in Fig. 5; the experimental uncertainties appear small enough to rule out such a model.

The foregoing considerations show only that the diffracted-intensity data seem incompatible with models containing no cyclic species. Because of experimental uncertainties, there remains the possibility that appreciable concentrations of chain-type species could exist together with cyclic

ones and not be discernible in the diffraction experiments. An important point to be noted here is that the arguments and conclusions of the preceding two paragraphs are strengthened rather than weakened if the true value of R should turn out to be less than unity owing to nonoptimum conditions such as multiple scattering in the comparatively dense sample jet.

Deficiencies of area[7] under Peak 1 raise the question of whether or not indices of resolution below unity are indicated. Peak 3 of the low-temperature f(r) curve furnishes an independent, internal estimate of the maximum possible cumulative lowering effect on R by all influences. An R value less than 0.84 does not seem reasonable, given that the area of the third low-temp. peak is only ∿5% uncertain and that the association factor does not exceed 5. It seems inconceivable that contaminants could have been introduced into the experiment in sufficient quantity to affect this conclusion. Nevertheless, even if appreciable contamination could have occurred, the most plausible impurities (air, water, and SiF_4) are incapable of accounting for the 20-30% amounts by which the first peaks appear to be deficient.

Theoretical fourth f(r) peaks for a few typical nearly-adequate trial models which were investigated are compared with experimental results in Fig. 6, where the inadequacies of these alternative models are evident. Characteristics of the model favored on the basis of the data are discussed below and are summarized in Table 5.

---

[7]See Subsection 4, pp. 49-50.

Fig. 6. Comparison of low-temperature experimental f(r) results (solid curves) with functions (dashed curves) computed for several typical trial models considered. With each trial oligomer, the model incorporated the proportion of monomer needed to make the obs and calc peaks at 2.5 Å match in area as nearly as possible, except with (a) the amount of monomer was taken as zero rather than the negative value which would have given a better fit to the 2.5 Å peak. The various experimental curves reflect slight influences in the direction of the respective trial models. These variations give rise to a degree of uncertainty which was taken into account in reaching the conclusions of this study.
(a) planar zigzag hexameric chain with tetrahedral FFF angles
(b) regular planar pentagon
(c) regular planar hexagon
(d) hexameric ring with 100° FFF angles and chair conformation
(e) hexameric ring with tetrahedral FFF angles and boat conformation
(f) hexameric ring with $102\frac{1}{2}°$ FFF angles and chair conformation
Although the fit in (f) is satisfactory, equally acceptable results are possible with a boat conformation and $105\frac{1}{2}°$ angles, or with other models having averaged conformation intermediate between these two extremes.

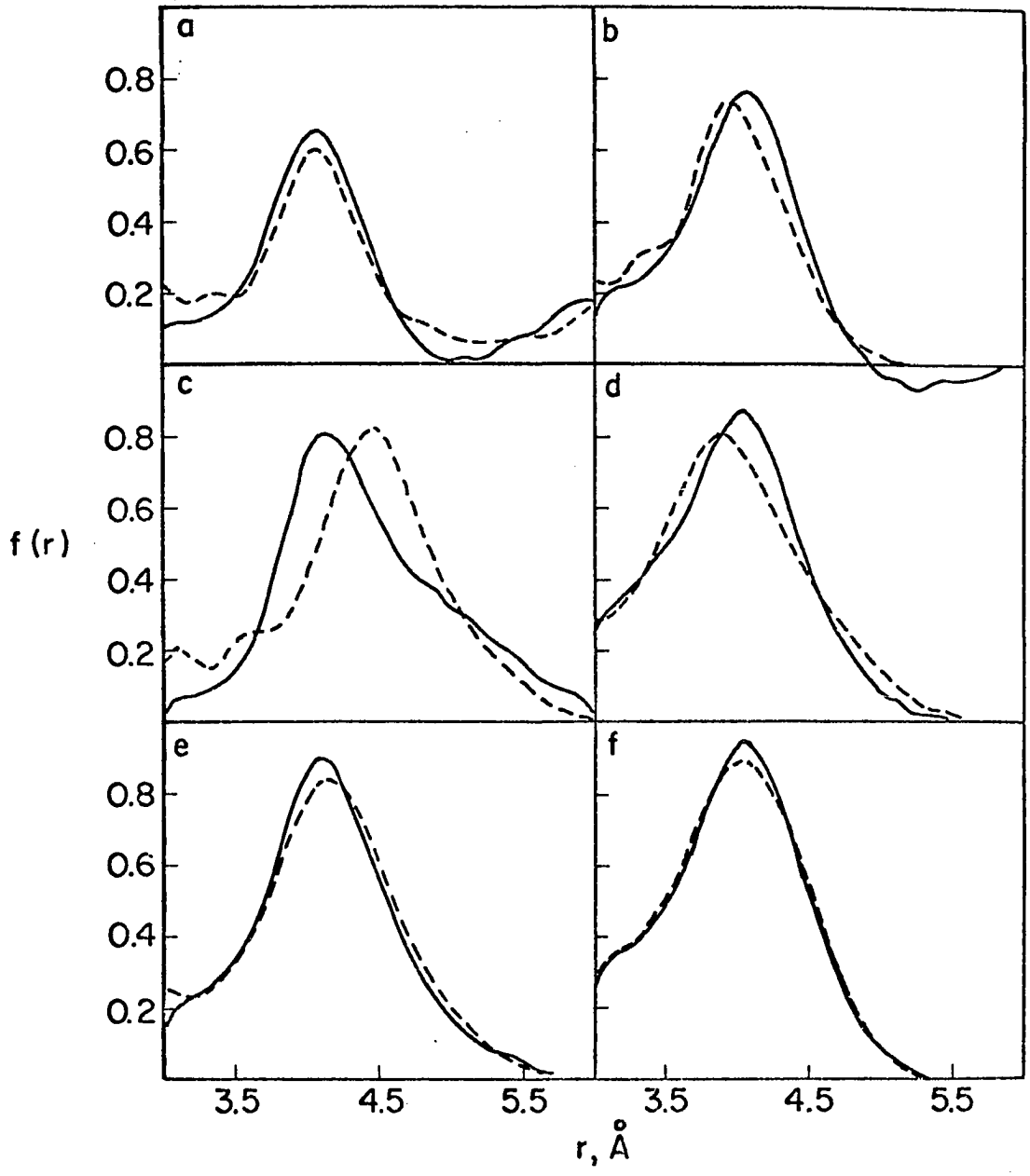
a
b
c
d
e
f
0.8
0.6
0.4
0.2
f (r)
3.5
4.5
5.5
r, Å

Table 5. Structural parameters from least-squares fitting of intensities

Temp. of sample cell	+22 °C	-19 °C
Sample composition	$4.2HF + (HF)_6$	$1.0HF + (HF)_6$
Association factor	1.96	3.50
$r_g(0)$ [F-H 1b][a]	0.973±.009 Å	0.973 .009 Å
Δr [F-H][b]	0.04_0±.009 Å	0.04_0±.009 Å
$r_g(0)$ $[F_1F_2]$[c]	2.535±.003 Å[d]	2.525±.009 Å
ℓ_m $[F_1F_2]$[c]	0.101±.003 Å	0.089±.003 Å
$r_g(0)$ $[F_1\cdots F_3]$[e]	3.88 ±.06 Å	3.94 ±.05 Å
ℓ_m $[F_1\cdots F_3]$	0.36 ±.06 Å	0.39 ±.06 Å
$r_g(0)$ $[F_1\cdots F_4]$[e]	4.40 ±.11 Å	4.37 ±.14 Å
ℓ_m $[F_1\cdots F_4]$	0.30 ±.10 Å	0.33 ±.08 Å
Anomalous protons[f]	34%	23%
Dimer contribution[g]	<3.5%	<0.6%

[a] Shortest FH distance in the polymer.

[b] Increase in above distance over monomer bond length.

[c] The $r_g(0)$ and ℓ_m notation is as in Ref. 50.

[d] A better f(r) fit is obtained if this distance is taken as 2.531 Å.

[e] Based on assumption of chair-type conformation.

[f] Deficiency in Peak 1 and surplus in Peak 2, percent of total hydrogens in sample.

[g] Contribution to polymer M(s), estimated from data in the literature.

1. Composition

The readily apparent enhancement of the molecular scattering features (Fig. 4) and f(r) peak areas (Fig. 5) which results from lowering the sample temperature is necessarily interpreted in terms of an increase in the degree of association, rather than a change in R associated with the reduction in sample pressure from the large value used at 22 °C; this conclusion follows from quantitative consideration of the f(r) peak areas. For each experimental temperature, Table 5 gives the proportions of monomer and cyclic hexamer deduced in fitting of the data. The corresponding association factors are both plausible values. Moreover, both are large enough to justify the neglect of aggregates other than the cyclic hexamer in analyzing the data, because the expected dimer contributions[8] are at or below the level of noise in f(r) and uncertainties in indices of resolution.

2. Hydrogen-bonded fluorine-fluorine distances

The dominant features of the diffraction pattern correspond to the 2.5 Å hydrogen-bonded FF distance, to be referred to hereafter as F_1F_2. This distance is well defined by the data and is in substantial agreement with the distance found in crystalline HF by x-ray diffraction (30). The mean distance and its vibrational amplitude may be slightly greater at the higher temperature.

[8]An examination (pp. 1-25) of the literature disclosed no compelling evidence for the existence, in vapors at equilibrium, of any other polymeric species which could make larger contributions. *Cf.* specifically p. 17, and also Abb. 12 of Ref. 18.

3. Non-hydrogen-bonded distances and configuration

The fourth f(r) peaks consist mostly of unresolved F_1F_3 and F_1F_4 components smeared out by large amplitudes of vibration. Near-zero restoring forces for $F_1F_2F_3$ angles are consistent with theoretical predictions (47, Fig. 2).

The average F_1F_3 distance corresponds to an $F_1F_2F_3$ angle of ∿104°, which is significantly smaller than the 120.1° angles found in the crystal structure (30), and which clearly disagrees with the value 140 ± 5° reported in the earlier electron diffraction study (10) for the apparent FFF amgle. In view of the large vibrations involved, sizable shrinkage effects (48) may be expected. It is possible that in the equilibrium configuration the ring of fluorine atoms is planar, with FFF angles the same as those found in crystalline chains. The amount of shrinkage necessary to reduce the apparent angle from 120 to 104° is of the order of only 9%, and shrinkages exceeding 3% have already been observed for comparably large distances in the presumably much more rigid C_3O_2 structure (49). Although the hexameric ring appears more "cyclohexane-like" than "benzene-like" in the mean distances it displays, insufficient information is available to distinguish boat, chair, or other conformations. It is probable, however, that a broad continuum of conformations is swept through as the exceedingly flexible ring vibrates.

Nonbonded FH distances greater than 2 Å and all HH distances give minor contributions buried in the f(r) peaks and cannot be deduced directly from the diffraction data. In the data analysis, approximate values for these distances were reckoned from the geometry of the fluorine skeleton

and were then formally included in computations to give consistent f(r) peak areas. The distance values used have no experimental significance, and errors therein do not appreciably affect the experimental outcome.

4. Distribution of fluorine-proton distances less than 2 Å

Structure parameters for the monomer were taken from the literature (50,51) and were not varied in the analysis. The monomer FH internuclear distance contributes to f(r) Peak 1; subtraction of the monomer contribution leaves a component (to be called Peak 1b) representing a slightly elongated (see Δr in Table 5) FH distance. The mean amplitude for the residual polymer component 1b does not differ from that ($\ell_\alpha = 0.065_2$ Å) of the monomer by more than the experimental error.

Relative to the expected[9] equal-multiplicity contributions to Peaks 1b and 2 by every proton in the oligomer structure, experimental Peak 1 is deficient in area by 34% at 22° and by 23% at -19°, while an apparently compensating amount of excess area appears in each case under Peak 2. If this area shift is genuine, the implication is that the average oligomer structure contains a sizable, temperature-dependent fraction of protons located in the region of space between two fluorines at a distance well beyond 1 Å from the nearest fluorine neighbor. According to this interpretation, Peak 2 would consist of three components. Unfortunately, an unambiguous resolution is not possible. Qualitatively, however, the center of gravity of the excess contribution to Peak 2 appears to be at more than half the F_1F_2 distance. This would imply large protonic excursions away

[9]See dashed curves of Fig. 5.

from F_1F_2 internuclear axes, and the observed anomalous peak area behavior is perhaps consistent with the existence of a low-lying secondary minimum in the potential energy field in which a H-bonding proton moves. In this connection it may be mentioned that spectroscopic properties of hydrogen bonds are not yet well understood and that large, unexplained temperature effects on infrared spectra have been reported previously (52,53). A relationship between the "tetramer bands" reported by Smith (13) and the "proton shift" under consideration here could conceivably exist, but has not been investigated. Not all aspects of the infrared and Raman HF crystal spectra have been accounted for (54), nor were the hydrogens located definitively in the x-ray study (30).

The results concerning shifts of area from Peak 1 to 2 are accepted with reservation because it is not impossible that experimental or interpretational complications are responsible. Attempts to devise plausible alternative explanations, however, have failed, leaving at least a strong possibility that, on the average, some of the FH bonded distances are severely stretched. If such is indeed the physical reality, the present experimental findings form an insufficient basis for attempting a theoretical explanation, but serve to underscore a need for further research into the question of how hydrogen-bonding protons are spatially distributed.

Conclusion

Electron diffraction does not by itself lead unequivocally to a unique solution for composition and molecular structure in self-associated hydrogen fluoride vapor, but the data are compatible with a model in which a cyclic hexamer exists as the predominant aggregate species. A similar

statement also applies to a body of physical evidence from other sources, which has been satisfactorily rationalized in terms of proposals made by Franck and Meyer (18). Taken together, the diffraction observations and data in the literature are mutually augmentative and strongly favor a ring-hexamer theory. Models consisting mainly of open-chain species, meanwhile, appear incapable of being brought into satisfactory accord with experimental observations. The dimer (24) could not be detected in this study, but would perhaps be observable in a room-temperature electron diffraction experiment if the working HF pressure were reduced to ∿200 torr.

Structural features of the hexameric rings are summarized as follows: The hydrogen-bonded FF distances are comparable with those found in the crystal. Mean FFF angles found by electron diffraction are roughly 16° smaller than those in crystalline chains, but in view of huge vibrations of an extremely flexible F-atom skeleton, the equilibrium angles do not necessarily differ from 120°. There is some indication that the distribution of protons in the polymer structure is not adequately describable in terms of a simple off-center placement of each proton on the internuclear axis between the two nearest fluorine neighbors, nor in terms of any one-dimensional oscillator.

AZEOTROPES OF HF WITH N_2O_3 AND NOF

Introduction

Seel, Birnkraut, and Werner (55) reported the synthesis of two new compounds by the reaction of liquid NOCl with HF in excess HF solution at -20 to -30 °C. Flat halts were observed at 68 and 95 °C in the bp *vs.* volume distilled curve for the reaction mixture; distillate collected during each halt could be repeatedly redistilled at the same boiling point without change in composition. Analyses by wet-chemical methods for nitrogen as NO and for fluorine gave results consistent with the formulas $NOF(HF)_6$ and $NOF(HF)_3$ for the fractions boiling at 68 and 95 °C, respectively. To the latter material could be added either HF or NOF, and the original fraction remained recoverable by normal distillation. It was later discovered (56), however, that the higher-boiling fraction suffered loss of HF in a vacuum, leaving an NOF-enriched residue of composition corresponding to $NOF(HF)_{2.5}$.

Seel and co-workers concluded that the three substances thus discovered were more or less stable complexes of HF with NOF. The question of molecular structure in such complexes was of sufficient intrinsic interest to warrant the undertaking of an experimental structure investigation. A study of the vapors by electron diffraction (e. d.) seemed appropriate because the formulas indicate reasonably small numbers of atoms per molecule and the vapor pressures lay in the convenient working range for e. d. experiments. This chapter concerns a series of diffraction measurements made to elucidate the nature of distillates from the NOCl-HF reaction mixture.

Partial results of work initiated in this laboratory have been reported previously (35). The reaction products have also been studied by Siegel (57): Extensive evidence from infrared, distillation, and wet-chemical analyses indicated that the 68° and 95° distillates are azeotropic mixtures instead of distinct molecular complex species. The 68° fraction appeared to be a maximum-boiling azeotrope having composition N_2O_3 + (12.6 ± 0.2)HF. No band attributable to NOF appeared in the infrared spectrum of the vapor, and an identical substance could be synthesized by simply condensing pure N_2O_3 and HF together in the same container in appropriate proportions. Siegel also found that the amount of 68° material produced in the NOCl-HF reaction diminished as the concentration of contaminants in the reactants was reduced. Production of the lower-boiling fraction could then be explained by either the known presence of up to 5% impurities as oxides of nitrogen in commercial NOCl or the reaction of NOF with water, which is known to give N_2O_3 below 0 °C. The material distilling at 95° seemed to be an azeotrope containing HF and NOF, plus a smaller amount of N_2O_3. If the formula is written as $a_1N_2O_3 + a_2HF + NOF$, analytical results obtained by Siegel and by Seel, *et al.* place the point (a_1,a_2) within the enclosed region of Fig. 7. Finally, Siegel's experiments indicated that vacuum distillation results in loss of HF from both the original 68°- and 95°-boiling materials.

The e. d. study to be described furnishes independent information from which can be drawn conclusions about the validity of the conflicting views on molecular species extant in the vapor phase. Unconventional aspects of the data analysis are also of interest.

Experimental

The materials reported to be $NOF(HF)_6$, $NOF(HF)_3$, and $NOF(HF)_{2.5}$ will for convenience be respectively designated hereafter as Substances I, II, and III. Two samples each of Substances I and II and one sample of III were furnished in sealed Kel-F tubes by Prof. Seel; diffraction photographs were made using the Iowa State University apparatus (33). Seals were broken and the Kel-F containers were attached to the diffraction unit inlet line under a dry argon atmosphere.

Photographs of the first sample (IIa) of II, and early plates of the first sample (Ia) of I were made using an inlet line of stainless steel and brass for injecting the vapors into the diffraction unit. Results obtained with this injection system could not be regarded as unambiguous because of a possibility that reaction with the walls of the sample system had decomposed the complexes of interest. Injection equipment consisting only of inert materials, namely Kel-F, nickel, Monel metal, and platinum, was therefore used to obtain photographs of the remainder of the Ia sample, and of fresh samples of all three substances.

It should be kept in mind that the vapors introduced into the diffraction chamber were those found above a liquid at the ambient laboratory temperature, not at the liquid's normal boiling point.

Analysis of Data

The basic theoretical expressions and methods of data reduction were similar to those described elsewhere (38,45,46,50). Parts of the analysis were facilitated, however, with the use of an intensity-matching least squares computer program which seeks a best fit by adjusting the propor-

Fig. 7. Implied limits of composition for Substance II (bp 95 °C). Analytical results obtained by Siegel and by Seel, *et al.* are compatible with the formula $a_1N_2O_3 + a_2HF + NOF$, where (a_1,a_2) is any point within the enclosed region.

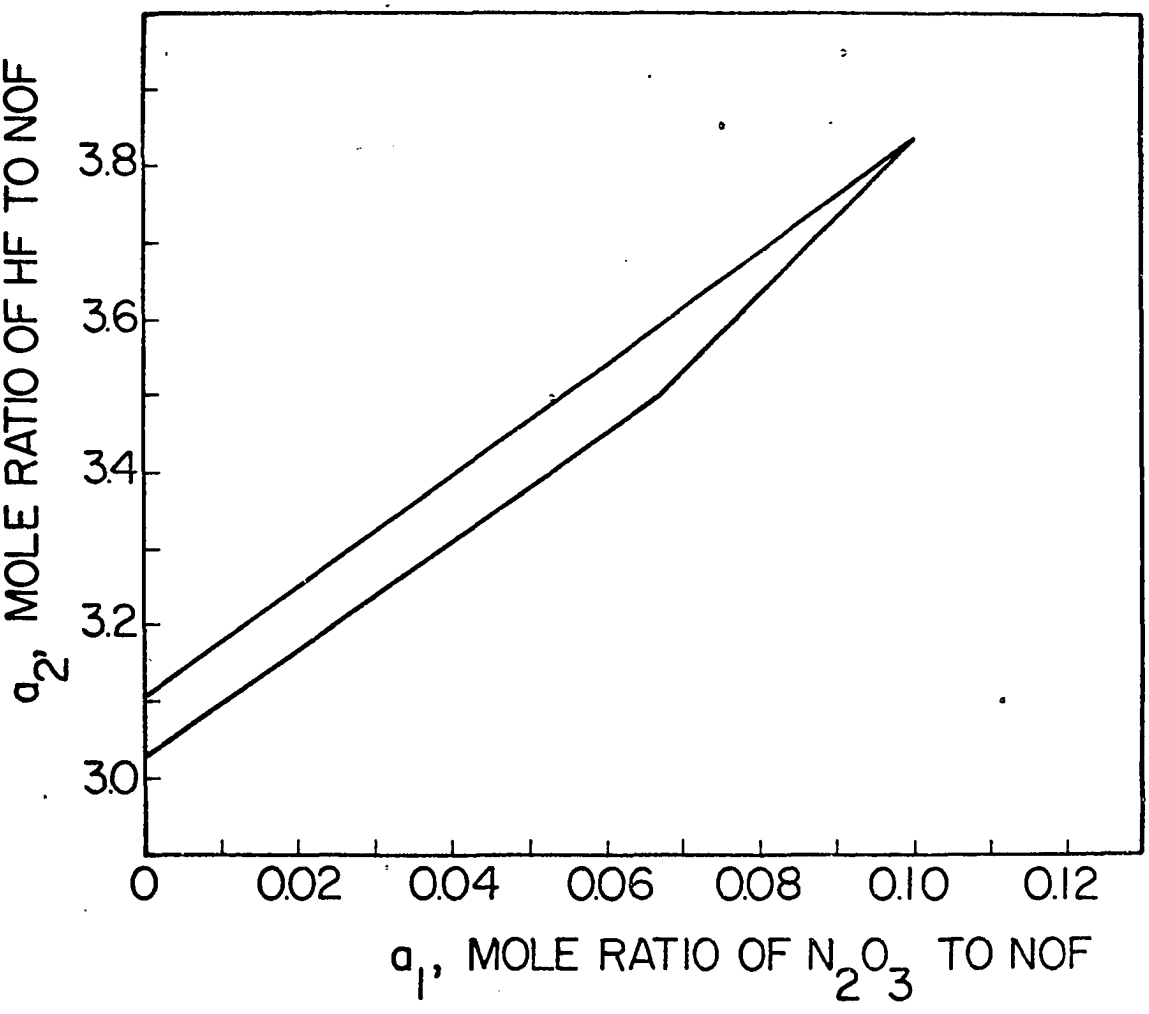
a_2, MOLE RATIO OF HF TO NOF
3.8
3.6
3.4
3.2
3.0
0
0.02
0.04
0.06
0.08
0.10
0.12
a_1, MOLE RATIO OF N_2O_3 TO NOF

tions of components in a mixture, given structural parameters for the component molecules and some starting guess at the composition. The applicable formalism is as follows.[1]

For a vapor which is a mixture

$$a_1C_1 + a_2C_2 + \ldots + a_jC_j + \ldots + a_JC_J$$

of J compounds C_j in mole-proportions specified by the a_j's, the resultant electron diffraction leveled intensity is computed from the reduced molecular intensity functions for the individual components. If for the single species C_j we define

$$A_j(s) = \sum[(Z - F)^2 + S], \tag{27}$$

where the summation is over the atoms of C_j only, and if we call the reduced molecular intensity of C_j alone $M_j(s)$, then the reduced molecular intensity for the mixture is

$$M(s) = (\sum a_jA_jM_j)/(\sum a_jA_j), \tag{28}$$

where each summation is from j = 1 to j = J, and a_J may be set equal to unity. For comparison with experiment, this M(s) can then be converted to a calculated leveled intensity in the usual[1] manner:

$$I_0(s) = B(RM + 1). \tag{29}$$

If the structures of the components are sufficiently well known that reasonably good $M_j(s)$ curves can be computed to start with, and if some initial estimate[2] of composition is available, then it is possible to

---

[1]Ref. 45 may be consulted for notation not defined here.

[2]*E. g.*, it was convenient to choose C_j to be the principal component and set the remaining a_j's to zero; this approach would be generally applicable in cases of slightly contaminated samples.

refine the composition estimate, along with a polynomial representation of the background function B(s), with a standard iterative least-squares technique. Such a calculation uses the derivatives

$$\partial I_0/\partial a_j = BRA_j(M_j - M)/(\sum a_j A_j). \qquad (30)$$

The number of constants R, a_1, ..., a_{J-1} which can be determined in practice is limited to at most the number of resolvable peaks in the experimental radial distribution curve, and may be smaller for reasons of molecular symmetry, *etc.* It was found practicable in this work to fix R at unity; it is then acknowledged that the usual few percent variation in R will be absorbed as uncertainty in the a_j's.

It was also found that, in case accurate structural parameters were not available in advance for all the likely constituents of a given vapor, alternate improvement of the composition and then of the structure could be continued in a cyclic fashion until self-consistency was reached.

Conventional radial distribution analysis (45) was also employed, and will be mentioned where appropriate.

Results

1. First vapors volatilized from Sample Ia

Figure 8 shows the leveled experimental intensity and background functions obtained from early photographs of the first sample of Substance I. Fourier inversion of these data leads to the radial distribution function f(r) shown in Fig. 9, which also shows the difference between the experimental f(r) and a theoretical function computed from the spectroscopic parameters (50,51) for HF monomer. Evidently unassociated HF was the only

Fig. 8. Leveled experimental total intensities and background functions for vapors volatilized early from Substance I. Solid and dashed curves refer to Samples Ia and Ib, respectively. All intensity data shown here and in subsequent figures were leveled and corrected for sector imperfections as described in Ref. 45, but have not been otherwise smoothed or adjusted.

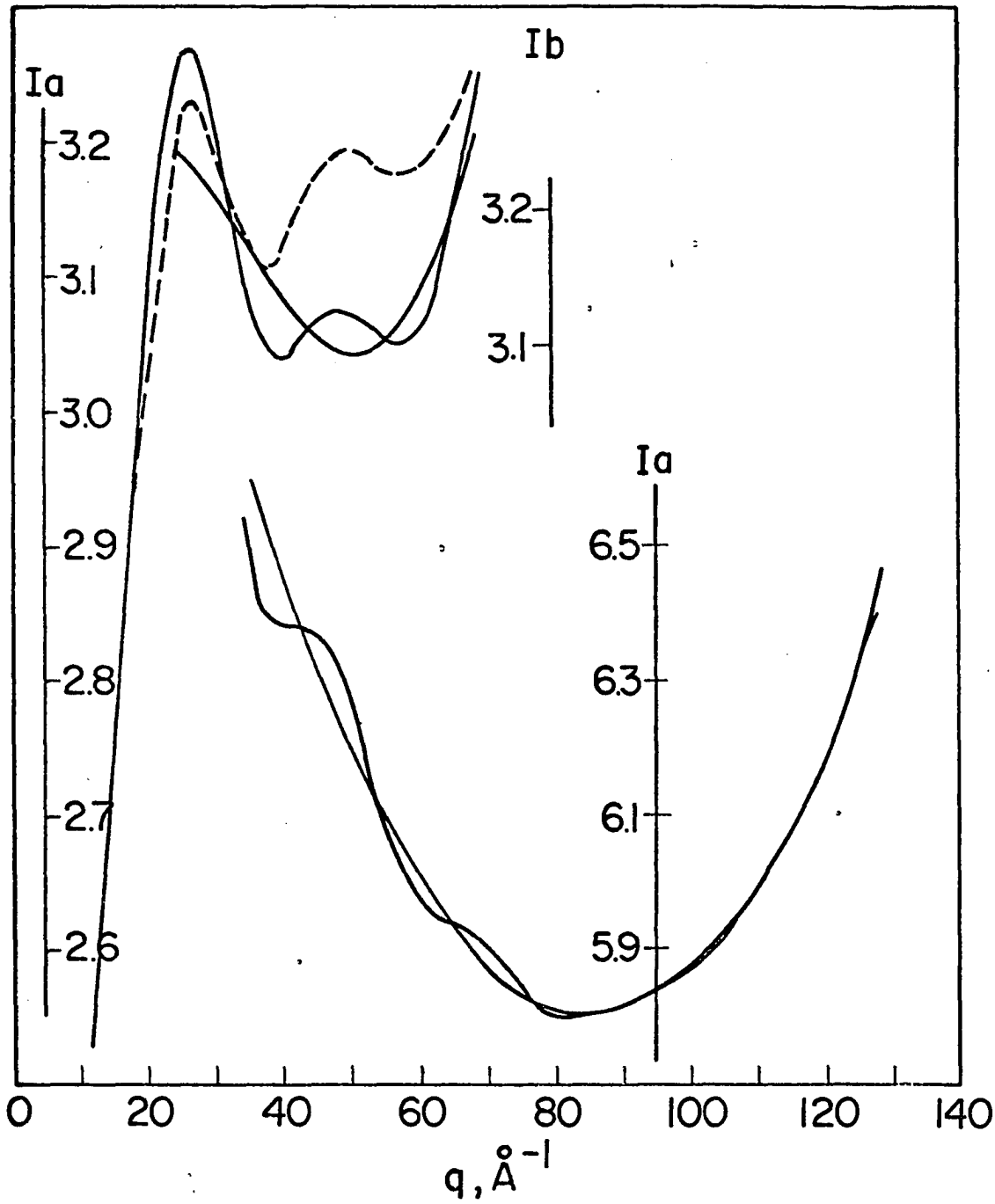
Ia
3.2
3.1
3.0
2.9
2.8
2.7
2.6
Ib
3.2
3.1
Ia
6.5
6.3
6.1
5.9
0
20
40
60
80
100
120
140
q, Å⁻¹

Fig. 9. Radial distribution function for Substance I in early stages of distillation

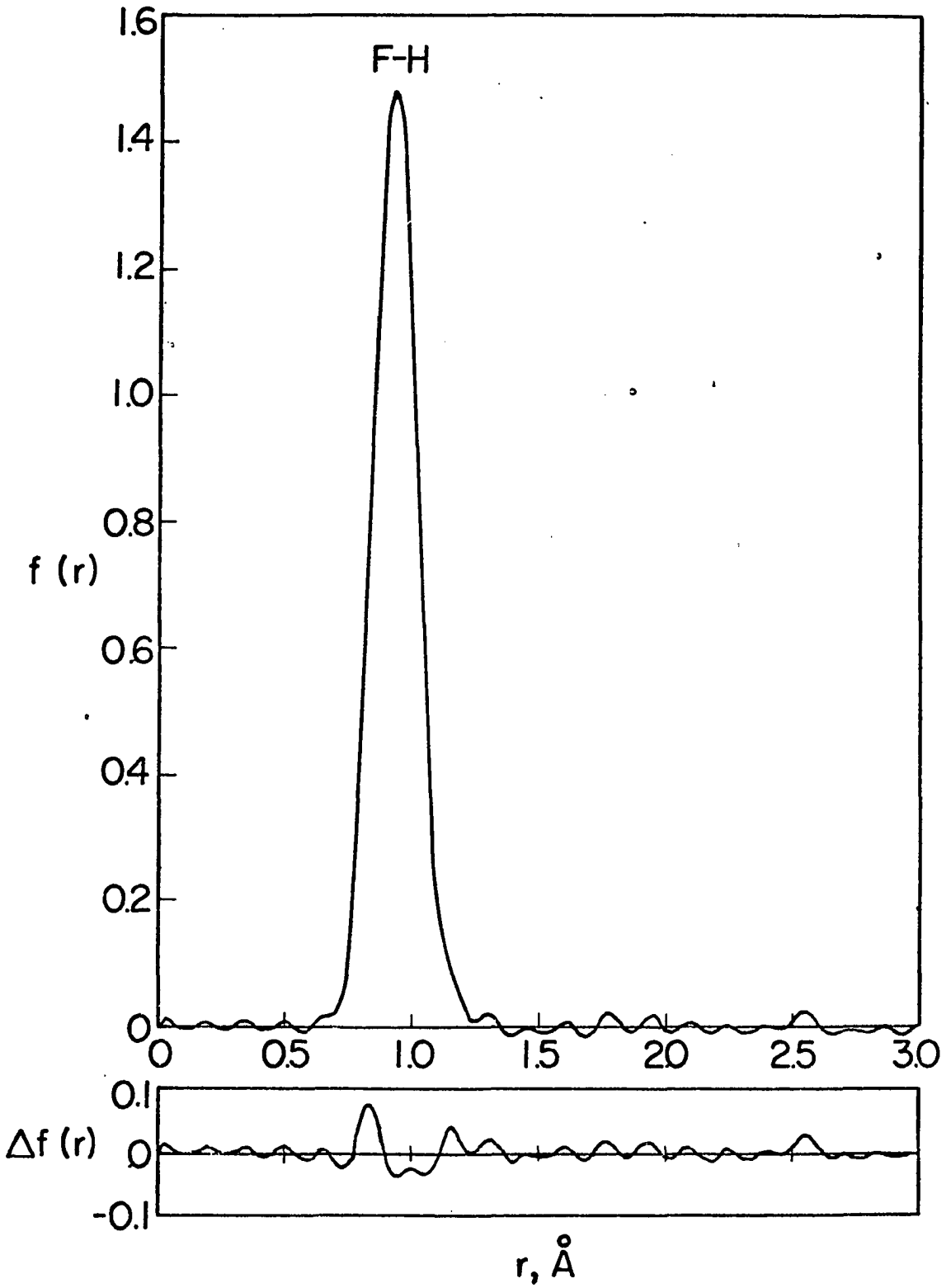
F-H
f (r)
1.6
1.4
1.2
1.0
0.8
0.6
0.4
0.2
0
0
0.5
1.0
1.5
2.0
2.5
3.0
Δf (r)
0.1
0
-0.1
r, Å

detectable vapor entering the diffraction chamber during the first Ia exposures.

2. Later stages of Ia distillation

After a switch to an all-Kel-F sample injection system, excepting only a platinum nozzle tip, Sample Ia gave the diffraction patterns depicted in Fig. 10. The corresponding experimental f(r) is shown in Fig. 11, along with the mismatch between the experimental curve and a theoretical f(r) computed for the mixture NO + NO_2 + 12.6HF. At room temp. and 1 atm, N_2O_3 is only about 10% associated (58). The total pressure in this experiment was less than 84 torr, so it is adequate to regard N_2O_3 as being dissociated into NO + NO_2 for purposes of computing theoretical diffraction patterns.

The experimental f(r) curve could not be fitted with a model mixing NOF with HF, even if a severe distortion of the NOF molecule were postulated. Except for the small shoulder at r ≈ 2.5 Å, there is no evidence of a peak in the range 2.3 < r < 3.5 Å which could correspond to a hydrogen-bonded distance and hence indicate the existence of a complex species. The shoulder at 2.5 Å is much too small to indicate appreciable complexing, and is probably due to self-association of the HF, whose partial pressure over the liquid may be estimated as about 72 torr. These data therefore lead to the conclusion that not only is this material (I) not a complex species which maintains its integrity in the vapor phase, it does not even appear to contain NOF in appreciable amounts. It is, rather, an N_2O_3 + 12.6HF azeotrope, as was also found by Siegel.

Fig. 10. Experimental intensities for Substance I in later stages of distillation. Solid and dashed curves refer to Samples Ia and Ib, respectively.

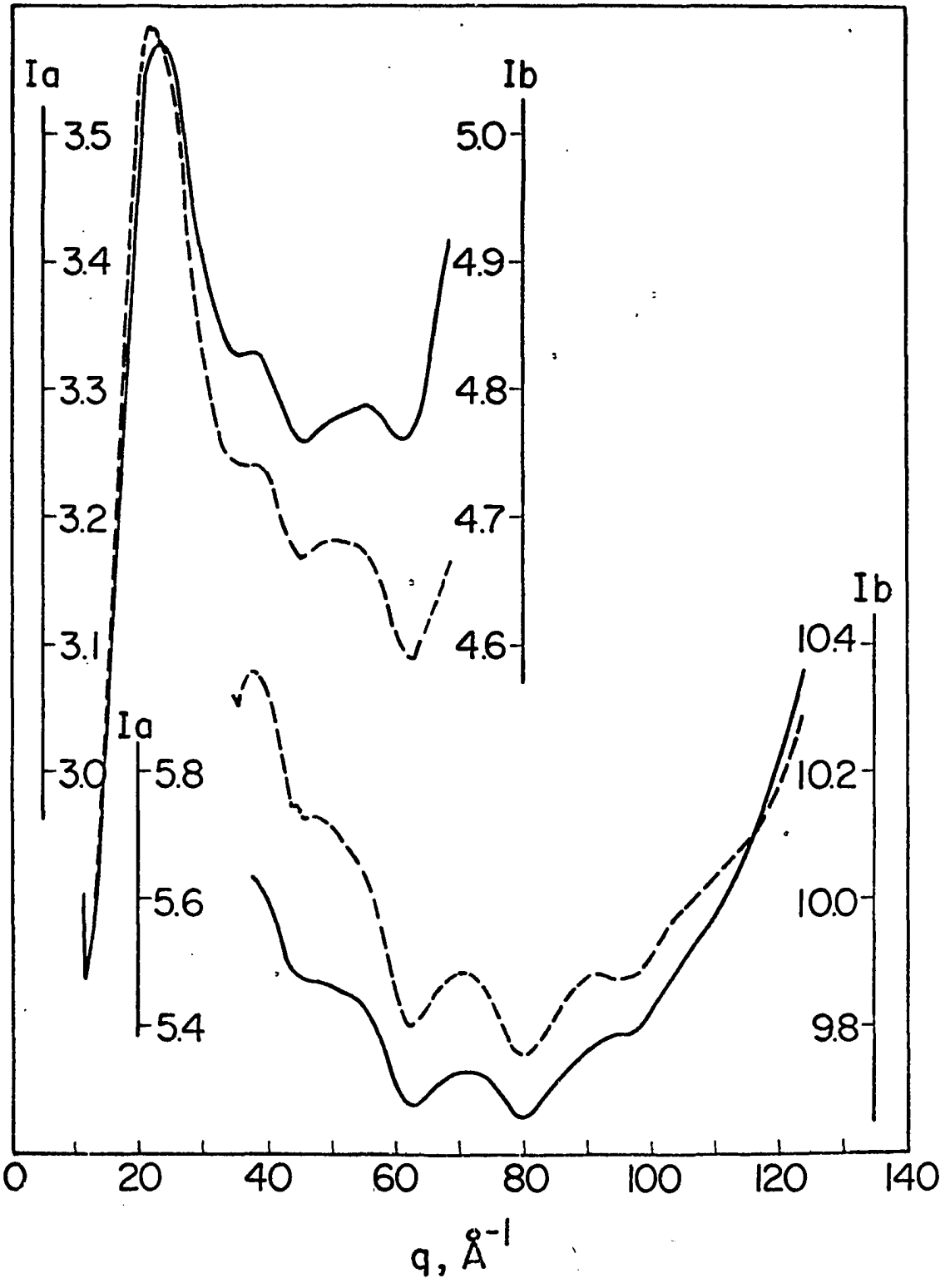
Ia
3.5
3.4
3.3
3.2
3.1
3.0
Ib
5.0
4.9
4.8
4.7
4.6
Ia
5.8
5.6
5.4
Ib
10.4
10.2
10.0
9.8
0
20
40
60
80
100
120
140
q, Å⁻¹

Fig. 11. Radial distribution function for later vapors from Substance I. Subtraction of a theoretical function calculated for the simple mixture NO + NO_2 + 12.6HF leaves the residual curve shown as $\Delta f(r)$. These results are from Sample Ia.

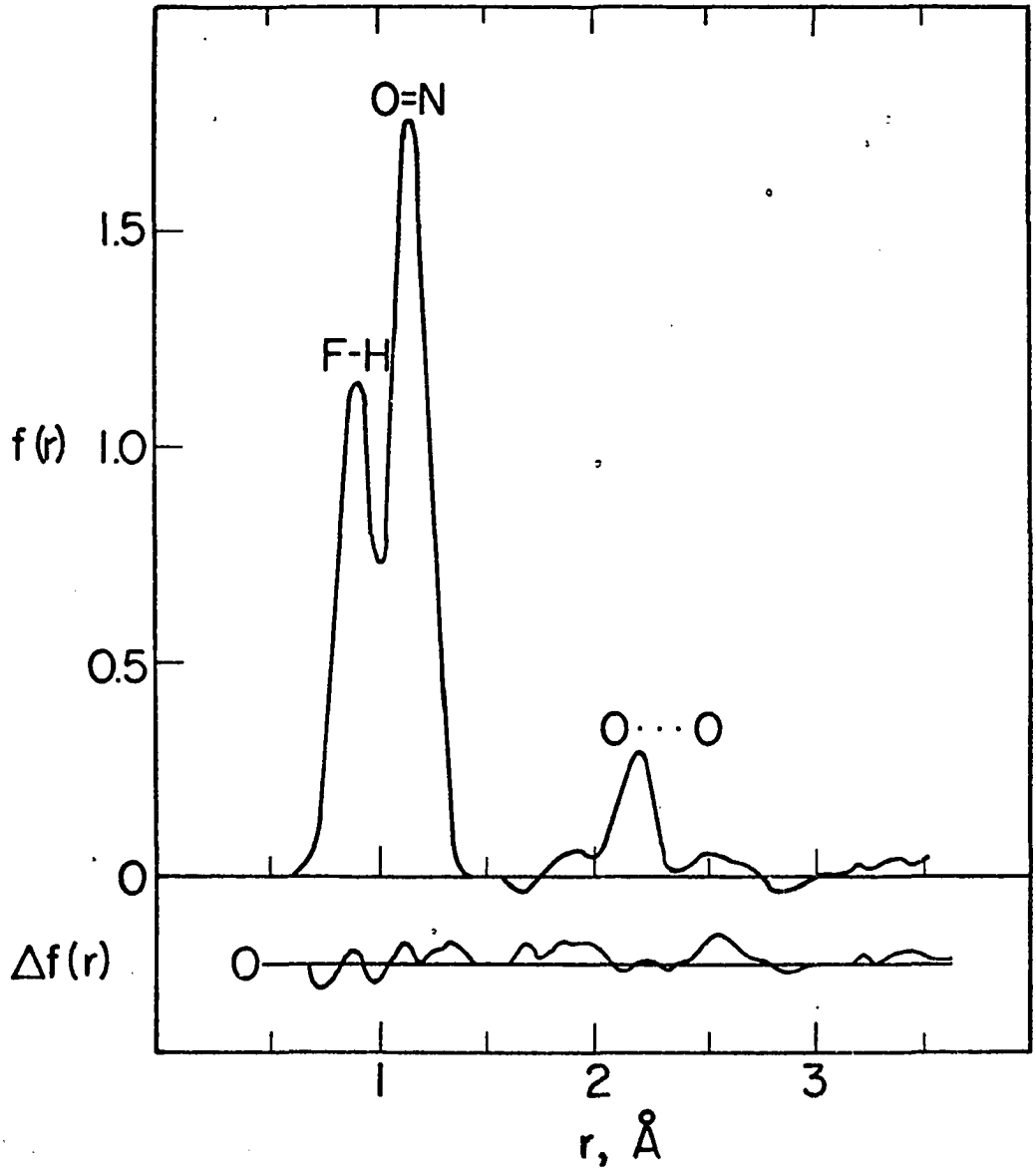
O=N
F-H
O···O
f(r)
1.5
1.0
0.5
0
Δf(r)
0
1
2
3
r, Å

3. Sample Ib

Independent verification of the above results was obtained by repeating the entire series of experiments starting with a fresh sample and avoiding possibly reactive container materials. Leveled intensities from early and from later plates taken with the second sample appear in Figs. 8 and 10, respectively. In each case, the molecular patterns can be seen by inspection to be essentially the same as in the analogous data from Ia; only the background functions are slightly different. Decomposition of the NOF-HF complex by reaction with the container walls is therefore not the explanation for the fact that the diffraction pattern changes as sample volatilization progresses nor for the fact that evidence for complex species was not found.

4. First sample of Substance II

Leveled intensities for Sample IIa are compared with the later Ia data in Fig. 12. It is evident that again the results are for a mixture of nitrogen oxides with HF in approximately the same proportions found in the case of Substance I.

5. Second sample of Substance II

Experimental difficulties resulted in the expenditure of perhaps 20% of the second sample (IIb) before usable plates were obtained. The opportunity to reproduce the results of the preceding paragraph was therefore missed. Data obtained for the remaining portion of IIb, however, are depicted in Fig. 12; curves for the three apparatus configurations used are numbered to show the temporal order in which the data were taken. It is

Fig. 12. Experimental intensities for Substance II.
The dashed curves are late Ia data from Fig. 10 included for comparison with IIa intensities. Note variation with extent of distillation from a pattern resembling the Substance I dashed curve toward the Substance III pattern of Fig. 13.

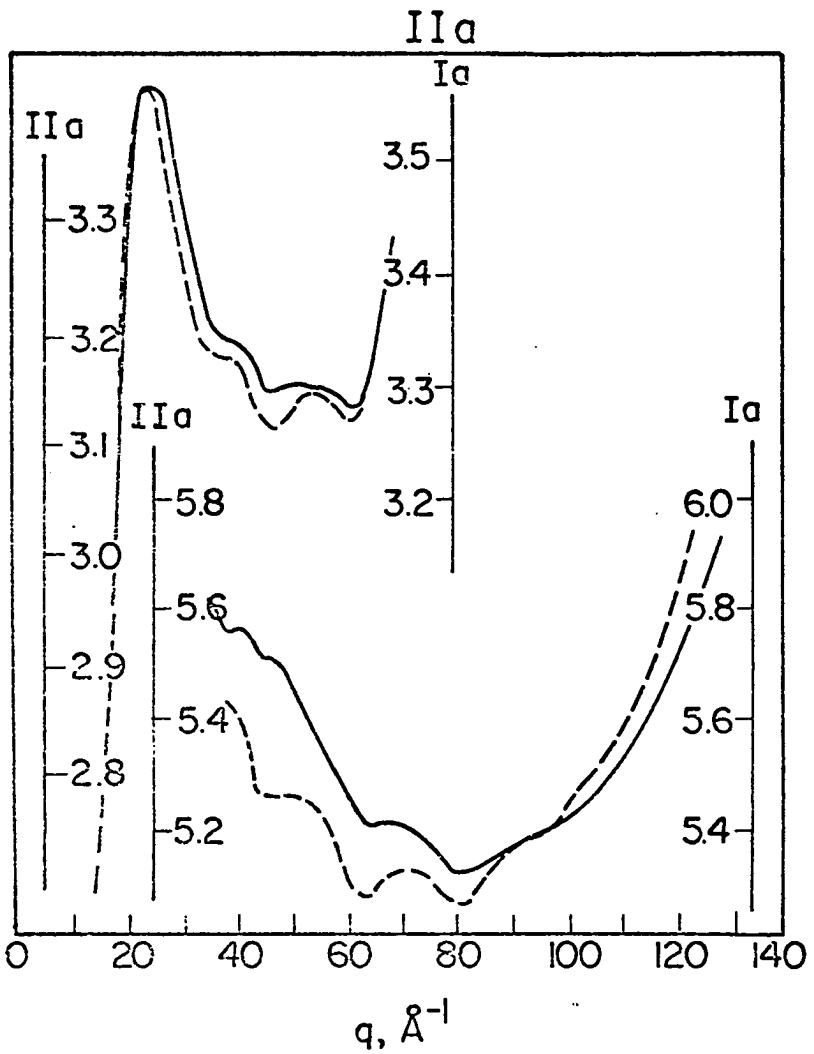
IIa
Ia
IIa
3.5
3.4
3.3
3.2
3.3
3.2
3.1
3.0
2.9
2.8
IIa
Ia
5.8
5.6
5.4
5.2
6.0
5.8
5.6
5.4
0
20
40
60
80
100
120
140
q, Å-1

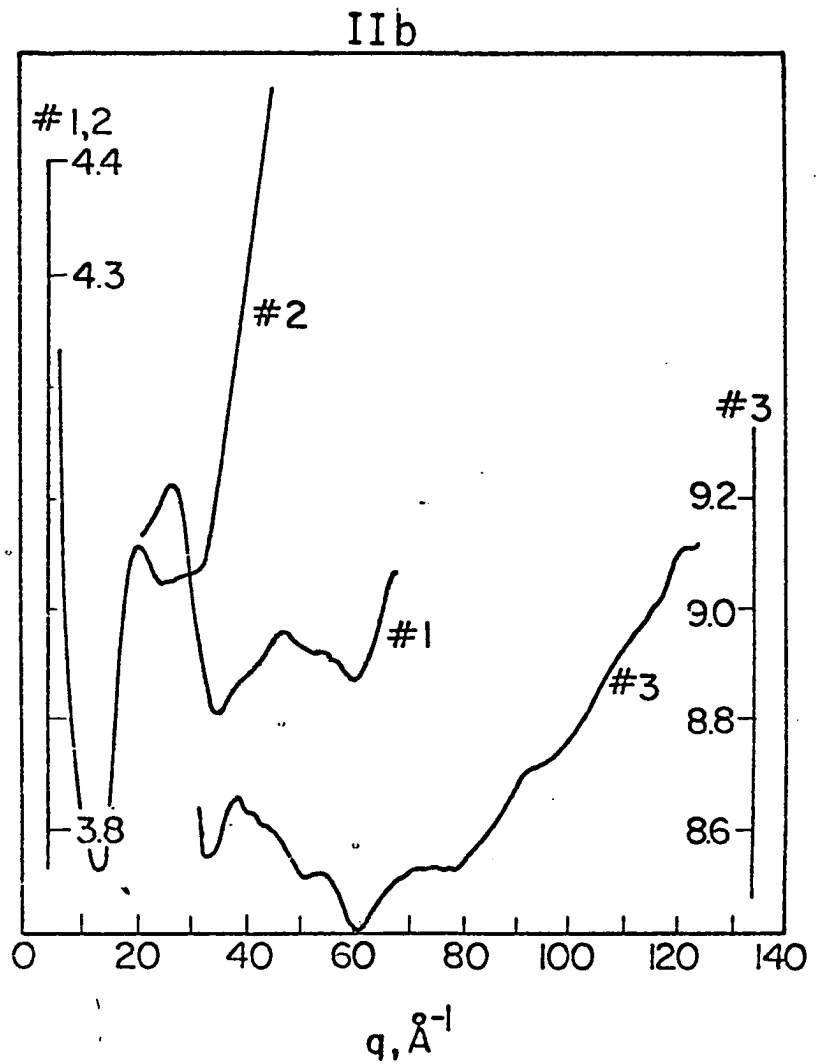
IIb
#1,2
4.4
4.3
3.8
#2
#1
#3
#3
9.2
9.0
8.8
8.6
0
20
40
60
80
100
120
140
q, Å-1

clear[3] that the pattern was changing as evaporation of the sample into the diffraction chamber progressed. Such behavior itself is not unexpected of an azeotrope being redistilled at reduced pressure and temperature.

It is possible to follow the changing composition of the vapor by fitting the leveled intensity curves individually. Curve #1 bears a strong resemblance to the pure HF data of Fig. 8; there are also visible, however, a few small ripples superimposed. Indeed, a good fit to this curve is obtained with the theoretical model NOF + 27.4HF. A less satisfactory fit, with rms deviation 3.4 parts per thousand *vs.* 2.5 for the foregoing model, was obtained using dissociated N_2O_3 for the minor component instead of NOF. The experimental data do not contain enough detail to justify the use of both NOF and N_2O_3 in the model.

In #2 and #3 the features of shorter period are more pronounced, indicating a larger ratio of NOF to HF; these two curves together are fitted satisfactorily using a mixture of averaged composition $0.12(NO + NO_2)$ + 6.6HF + NOF.

The e. d. data imply, then, that Substance II is an azeotrope of NOF and HF in the approximate composition indicated by the formula $NOF(HF)_3$, but containing also a little N_2O_3 (*cf.* Fig. 7). Vacuum distillation results in preferential loss of HF, accompanied at first (IIa) by N_2O_3 in amounts such that essentially Substance I is obtained. Under continued pumping, the sample next (IIb, #1) loses HF along with less than 1/25 mole of NOF per mole of HF. As vaporization continues further (IIb, #2,3), NOF

---

[3]Note, for example, that at q ≈ 28, a maximum in #1 coincides with a minimum in #2.

continues to distill with a decreasing relative amount of HF, plus perhaps 0.1 mole of N_2O_3 per mole of NOF.

6. Substance III

Intensity results for III are shown in Fig. 13; the experimental f(r) curve is plotted in Fig. 14. Figure 14 also shows that a theoretical function for the mixture $0.12(NO + NO_2) + 2.15HF + NOF$ is decidedly better than that calculated for NOF + 2.5HF. Here it is again easily seen that there appears no evidence, as peaks in the hydrogen-bonded distance region from 2.3 to 3.5 Å, for the existence of any new complex molecules.

The sample of Substance III, expected to be a vacuum distillate obtained after loss of HF from II, evidently was just that: The composition of the samples IIa and IIb, it was shown above, appeared to be changing in the direction of the composition found for III.

Structural parameters available from the literature (59-62) for NOF are less precise than those for HF, NO, and NO_2 (51,63,64). It is possible to get structural information for this compound from the data of Figs. 13 and 14; it is a major constituent in Substance III. However, the O=N and N-F f(r) peaks are overlapped by the HF and NO peaks of the other components. Because the composition is also an unknown in the experiment, the structure parameters derived from these data have larger uncertainties than usual. The diffraction data do not disagree with the microwave results, but they are probably no more accurate, either: Refer to Table 6.

Discussion

The e. d. results for samples reported to be $NOF(HF)_6$, $NOF(HF)_3$, and

Fig. 13. Experimental intensities and background functions for Substance III

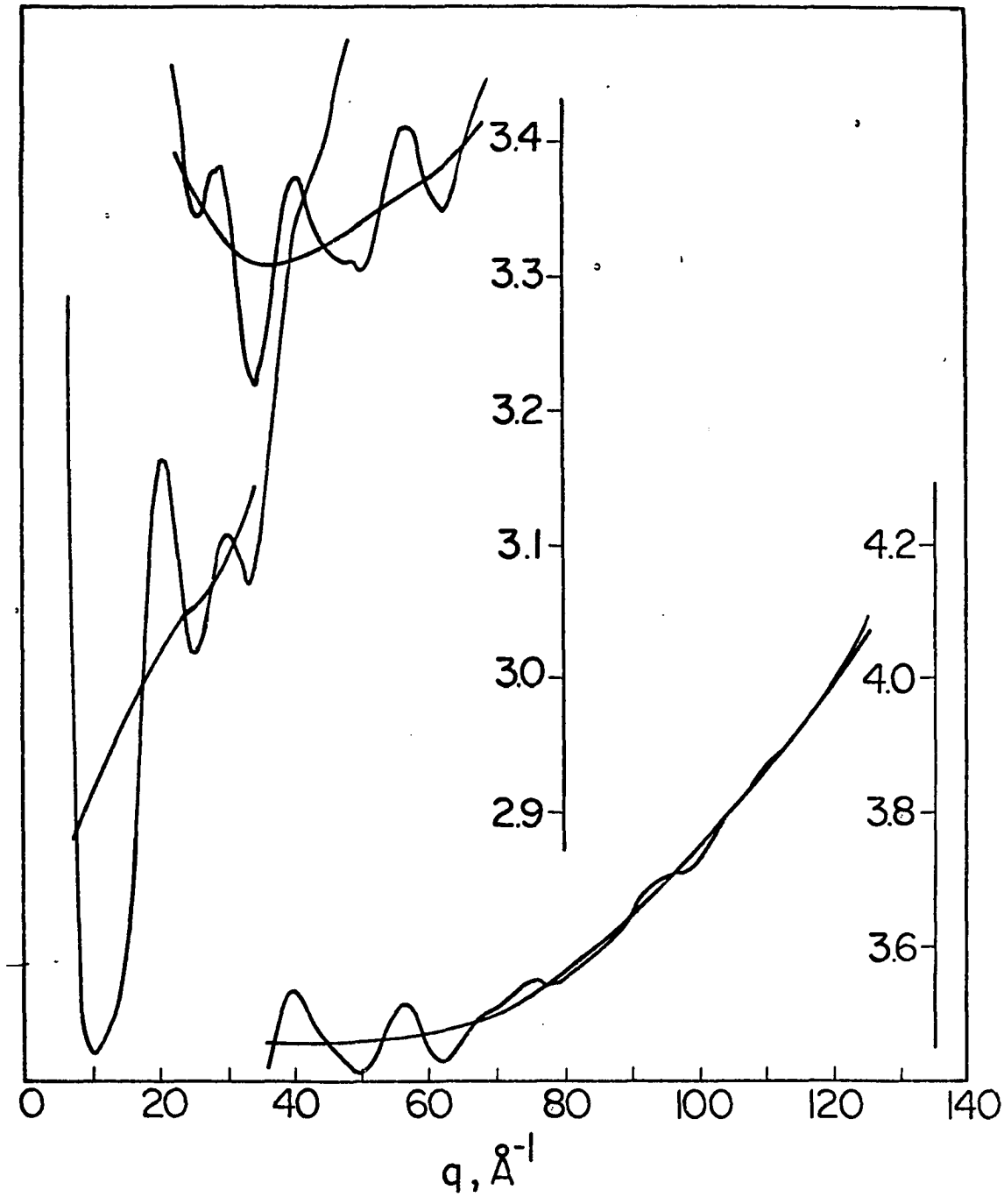
3.4
3.3
3.2
3.1
3.0
2.9
4.2
4.0
3.8
3.6
0
20
40
60
80
100
120
140
q, Å⁻¹

Fig. 14. Comparison of experimental f(r) for Substance III with functions calculated for NOF + 2.5HF (dashed curve, top) and for 0.12(NO + NO_2) + 2.15HF + NOF (dashed curve, bottom)

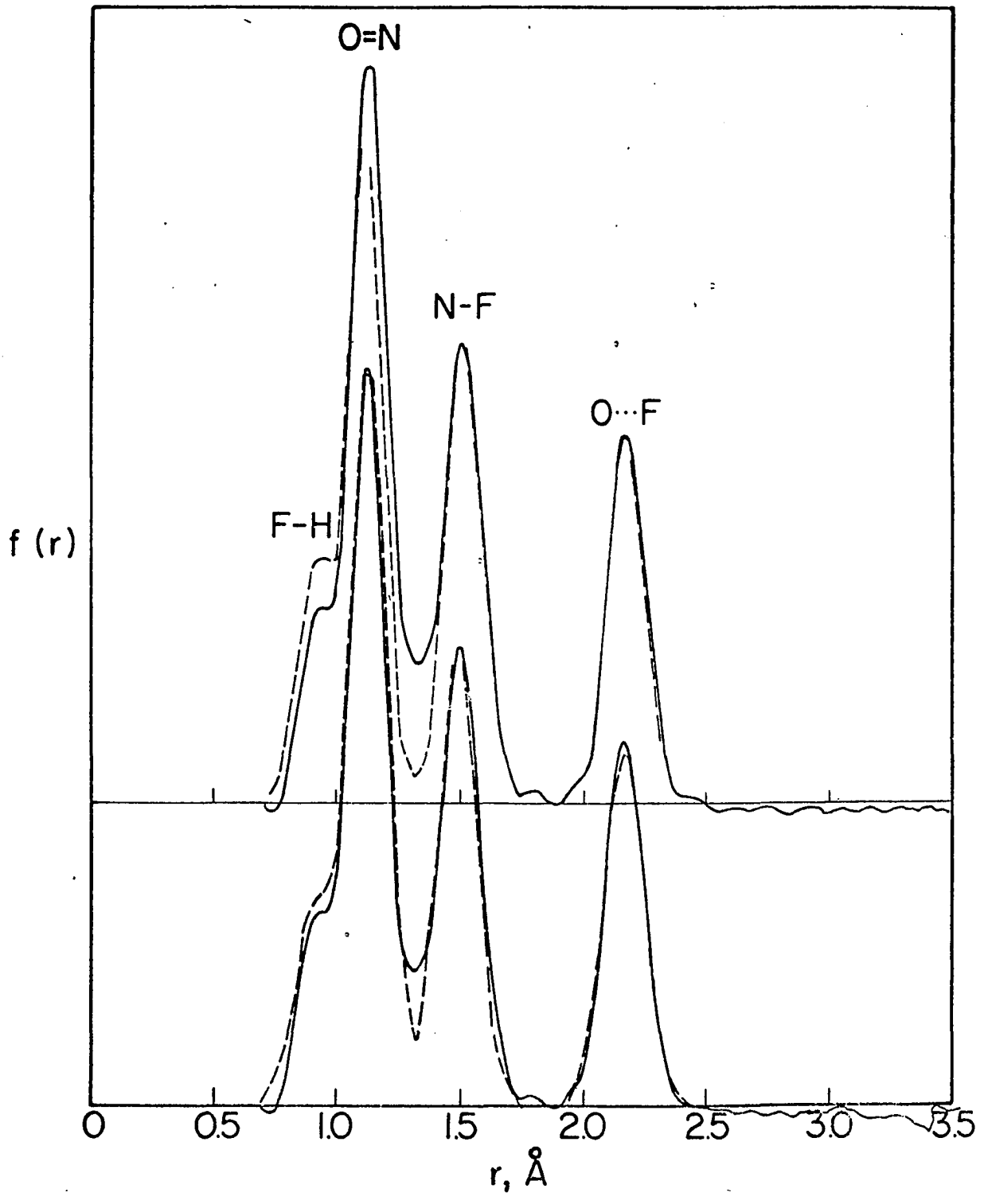
O=N
N-F
O···F
F-H
f (r)
0
0.5
1.0
1.5
2.0
2.5
3.0
3.5
r, Å

Table 6. Internuclear distances in nitrosyl fluoride

Distance	Electron diffraction[a]	Microwave[b]
O=N	1.14±.01 Å	1.13 Å
N-F	1.51±.01 Å	1.52 Å
O···F	2.18±.01 Å	2.18 Å

[a]Values are $r_g(1)$ parameters, in the notation of Ref. 50.

[b]Refs. 59,60.

$NOF(HF)_{2.5}$ are on every point in accord with observations made by Siegel; his description of these materials as azeotropic mixtures is confirmed.

The time required for a molecule to reach the electron beam after exiting the nozzle orifice into the diffraction chamber is estimated to be of the order of 1 μsec for the present experiments. HF polymers are easily detectable under comparable conditions (10), and it does not seem probable that true complexes stable enough to undergo distillation unchanged would be so much more labile than HF in a vacuum that they would escape detection in the present experiments.

The diffraction results, of course, pertain only to the vapor phase, and do not detract from the interesting properties possessed by the liquids as highly associated, potentially useful fluorochemical solvent-reagent systems, nor do they shed any light on the strong intermolecular interactions which seem to be indicated by the observed large departures from Raoult's law: Compare 68° and 95° with the HF, N_2O_3, and NOF boiling points 19.54, 3.5, and -60 °C, respectively.

It seems likely that the chemical reactions formulated in terms of $NOF(HF)_n$ complexes by Seel, Birnkraut, and Werner (55) can for the most part be rewritten as reactions of the constituents NOF, HF, and N_2O_3, although solvation effects by molecules not actually reacting may of course be important.

As an analytical tool, electron diffraction is yet too cumbersome for routine use. The experience of this study shows, however, that the technique is capable, in favorable cases, of being sensitive to rather subtle structural features while serving simultaneously to yield chemical analyses of mixed vapors. This capability may prove to be invaluable in future investigations.

NOTES ON PHOTOGRAPHIC-MICRODENSITOMETRIC MEASUREMENT OF ELECTRON INTENSITIES

Introduction

Commercially available equipment for the direct digital measurement of photocurrents presently enables workers in gas electron diffraction to rapidly make optical density measurements with better than 0.1% precision (65,66). The photometric apparatus in this laboratory has recently been updated to take advantage of the improved reliability, linearity, stability, and response speed offered by such equipment. It seems worthwhile to summarize some of the performance characteristics of the system[1] with which over-all microphotometric precision of a few hundredths of one percent is routinely achieved in our diffraction studies, and to comment on some implications thereof.

Accurate characterization of slight nonlinearity in the response of photographic emulsions to exposure with fast electrons has remained a problem lacking a wholly satisfactory solution. Some of the difficulties in calibrating emulsions can be overcome and usable results obtained by a method the principal feature of which is a refined computational procedure for analysis of calibration data. Recent experience in applying this method toward solution of the emulsion calibration problem deserves a few remarks.

---

[1]Similar systems are also in use elsewhere; a typical description appears in Ref. 66.

Microphotometer Performance

1. Apparatus contribution to random noise level

Standard random errors representing the practical limits of precision attainable with the present hardware, meaning microphotometer plus photographic plate, were empirically determined for various optical densities in the range from 0.075 to 1.9. Transmitted light readings were taken using a plate[2] mounted as usual in the microphotometer and spinning at 3.00 rps about the center of its diffraction pattern. Such data were recorded for a particular density with the optical system slit stationary at a fixed distance from, and always on the same side of, the spinning plate's center. Any reproducibility-degrading effects which might be due ordinarily to irregular motion of the plate as it is translated past the slit in the scanning process or to error in locating the center of rotation as a bench mark on the instrument's distance scale were therefore absent. Effects of any appreciable drift in the light source intensity or detection circuitry were also excluded by taking readings in sets, each set within a time period short in comparison to the drift rate of the instrument. The results obtained therefore express only the optimum reproducibility of a single density measurement made at a fixed radius on a spinning plate.

The relative uncertainty $\delta D/D$ in an optical density value

$$D = \log (V_1 - V_0) - \log (V - V_0) \tag{31}$$

is easily obtained by a conventional differential error computation as a function of the uncertainties in the three measured quantites V_1, V_0, and

---

[2]All results reported in this chapter refer to Kodak Process Plates developed in Kodak D-11.

V, which are voltages proportional to photocurrents obtained, respectively, at full-scale lamp intensity, with shutter closed, and with the absorbing medium of interest positioned in the light beam. The relevant expressions are

$$(\delta D)^2 = (\delta V_1 \partial D/\partial V_1)^2 + (\delta V \partial D/\partial V)^2 + (\delta V_0 \partial D/\partial V_0)^2, \quad (32)$$

$$\delta D/D = D^{-1} \log e\{[\delta V_1/(V_1 - V_0)]^2 + [\delta V/(V - V_0)]^2 + (\delta V_0)^2[1/(V_1 - V_0) - 1/(V - V_0)]^2\}^{\frac{1}{2}}, \quad (33)$$

and

$$(\delta V_i)^2 = [\sum (V_i - n^{-1}\sum V_i)^2]/[m_i(n - 1)] \qquad i = 0,1. \quad (34)$$

Replicate (n = 11) 10-second voltage readings were taken with the shutter closed and with the beam unobstructed by the plate; these readings were used to estimate the variances $(\delta V_0)^2$ and $(\delta V_1)^2$ using Eq. 34 with $m_0 = m_1 = 1$. Variances $(\delta V)^2$ in V(T) were similarly determined at various values of the transmission

$$T = (V - V_0)/(V_1 - V_0) \quad (35)$$

using both 10-second and 1-second counting periods. Values of $\delta D/D$ based on these observed variances were calculated according to Eq. 33 and the results are depicted in Fig. 15. The computations were repeated with $m_0 = m_1 = n$ to take account of the fact that in the normal operation of the instrument, V_0 and V_1 can conveniently be taken as means of several observations, so their uncertainties are correspondingly reduced. This second set of calculations gives results (Fig. 16) which are predictably somewhat below those of the $m_0 = m_1 = 1$ case when the counting time is 10 sec; the differences are insignificant for V(T) counting times of 1 sec because the dominant contribution to $\delta D/D$ then comes from $(\delta V)^2$. The

Fig. 15. Optimum relative error of optical density measurements with $m_0 = m_1 = 1$

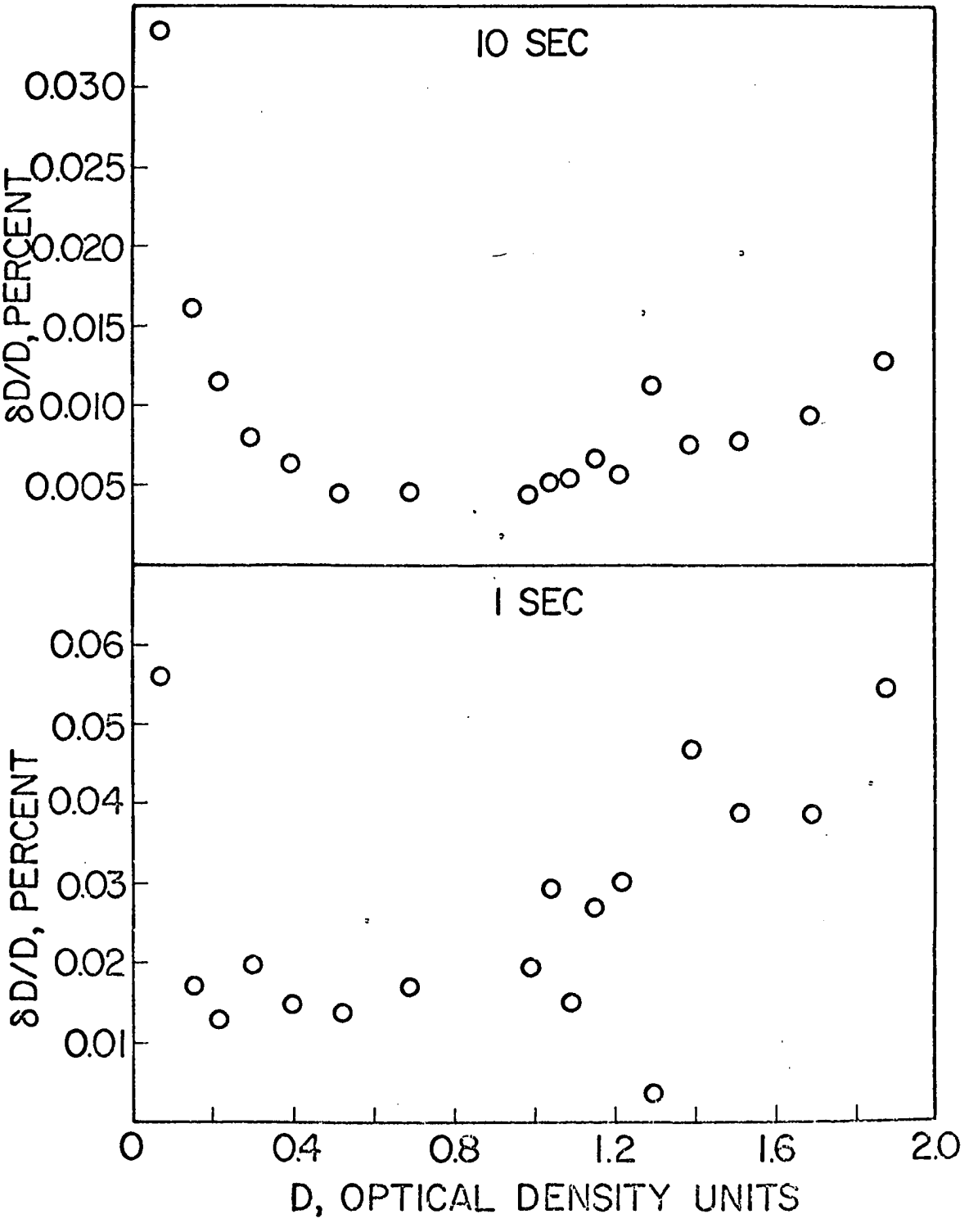
10 SEC
0.030
0.025
0.020
0.015
0.010
0.005
δD/D, PERCENT
1 SEC
0.06
0.05
0.04
0.03
0.02
0.01
δD/D, PERCENT
0
0.4
0.8
1.2
1.6
2.0
D, OPTICAL DENSITY UNITS

Fig. 16. Optimum relative error of optical density measurements with $m_0 = m_1 = 11$. The continuous curve is a plot of the function $(\log e)(-10^{-4}/e)/(T \log T)$.

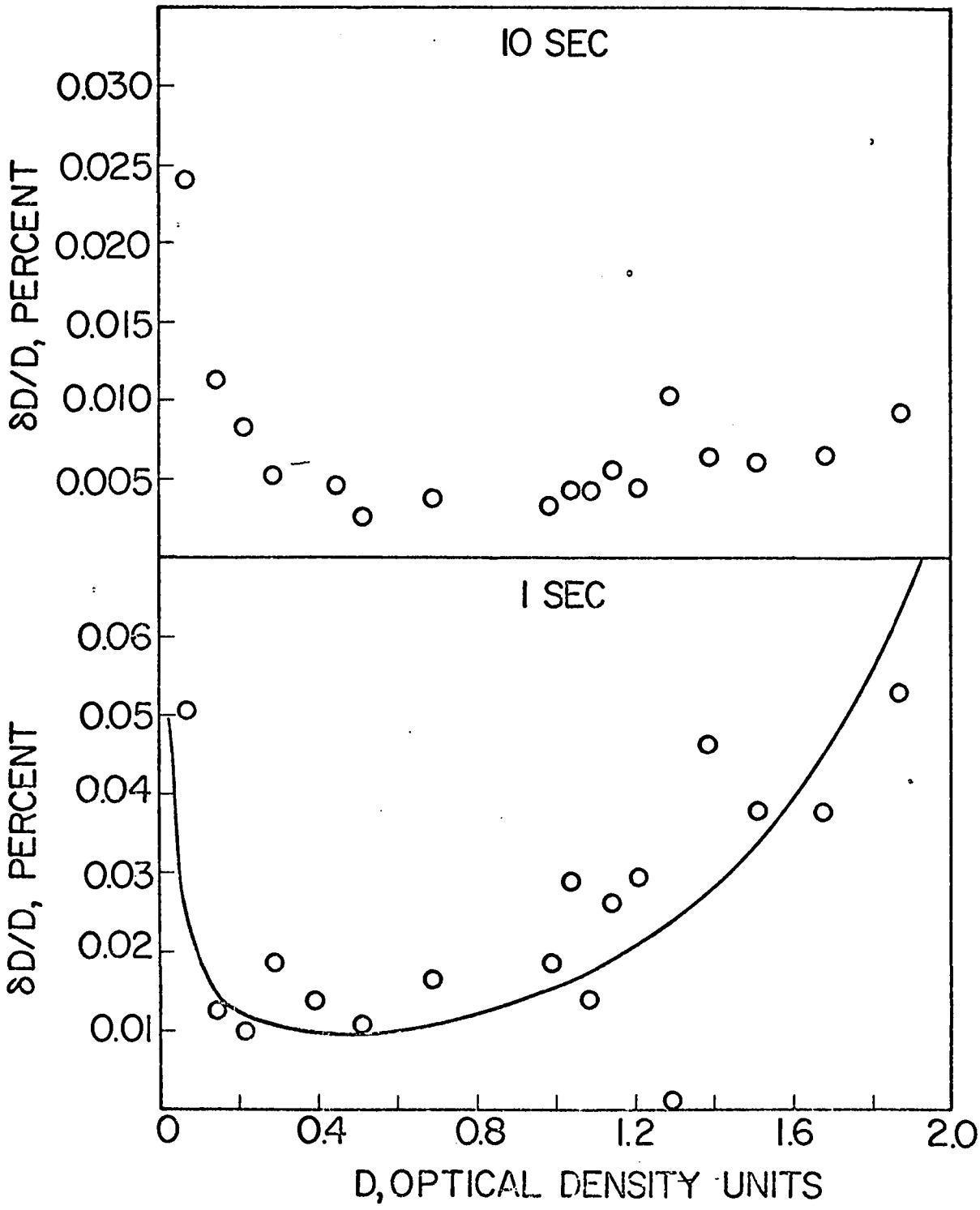
10 SEC
0.030
0.025
0.020
0.015
0.010
0.005
δD/D, PERCENT
1 SEC
0.06
0.05
0.04
0.03
0.02
0.01
δD/D, PERCENT
0
0.4
0.8
1.2
1.6
2.0
D, OPTICAL DENSITY UNITS

experimental results resemble the theoretical (67) error curve

$$\delta D/D = (\log e)\delta T/(T \log T) \qquad (36)$$

reckoned with δT a constant: A plot of this function, with scale arbitrarily fixed by taking δT as $-10^{-4}/e$, is included in the bottom half of Fig. 16 for comparison.

Of the four sets of results depicted in Figs. 15 and 16, the last is of principal interest here because it most nearly represents a standard operating procedure whereby a series of plates can be read at 1/8-mm intervals in a total time averaging 20 minutes per plate, not counting instrument warmup. The optimum working density range is evidently from roughly 0.3 to about 1.0, but it may be noted that densities as great as 2.0 are measureable with better than 0.1% precision.

If it may be assumed that Kodak Process Plates are no slower than Kodak Electron Image Plates, for which absolute sensitivity data are readily available (68, p. 12d), then the microphotometric precision indicated by the results in Figs. 15 and 16 approaches the statistical uncertainty of counting the number of electrons falling in the plate area scanned by the microphotometer slit during a typical reading. For a counting standard deviation of 0.01%, 10^8 electrons are necessary. A density of 1.0 in a circular band of width 90 μ and radius 44 mm would represent just $1.2(10^8)$ electrons at an absolute emulsion sensitivity of 0.2 density unit·μ^2/electron. The statement by Morino, *et al.* (65) that the ultimate accuracy of photographic electron intensity detection appears not very distant from present levels therefore seems to be in order.

The advantage gained in the averaging process which is accomplished by spinning the plates can be appreciated by comparing the indicated precision

of near 0.01% with Kodak's specification of the Process Plates' rms granularity as 1.4% (68, p. 11d).

2. Reproducibility under normal operating conditions

In addition to short-term random noise of the sort discussed in the preceding subsection, there are contributions of at least two other kinds to the microphotometric uncertainty as measured by $\sigma(D)$.[3] The first kind may be described as errors due directly to circuit lag and hysteresis, plus whatever intermediate-term meandering occurs about the linear, long-term course of drift for which a correction is made. The second kind may be classed as plate-positioning errors, whose contribution to $\sigma(D)$ is of course magnified to the extent that instrumental characteristics responsible for errors of the first kind can also introduce a systematic left-right difference by interfering with accurate location of the center of rotation of a spinning plate.[4] Before the most recent alterations in the equipment used in this laboratory, the combined effect of these contributions resulted in $\sigma(D)$ values approximately an order of magnitude larger (34, pp. 9,11; 35, p. 22) than the $\delta D/D$ results indicated in the bottom half of Fig. 16. With the present system, plate centers can be located to within 1 μ, which is of the order of 1% of the effective width of the scanning slit, and it is encouraging to note that the routine plate scanning process now gives duplicate density values which indicate reproducibility[5] comparable

---

[3]Refer to Eq. 23 on p. 31.

[4]Averaging of data from the two sides of a plate effectively cancels this systematic error from the final density results.

[5]See, for example, the $\sigma(D)$ values for -19° HF in Table 4 on p. 29.

with the optimums depicted in Fig. 16. It seems reasonable to conclude that noise contributions from plate-positioning errors and the various instrumental nonlinearities can be routinely held to negligible levels and that precision of the over-all densitometric procedure is now nearly all that can be justified within the limits of electron counting statistics. It also seems clear that plate-to-plate variations in recorded diffraction pattern shape are presently a source of significantly more statistical uncertainty than is the microphotometric measurement process.

Emulsion Calibration

1. Gross fog

The sensitivity of Kodak Process Plates has been found (41,43,44) to increase centrifugally beginning at about 24 mm from the center of a plate. The increase varies among individual plates, but typically amounts to about 5% near the outer edge (39). Gross fog (68, p. 5) data obtained from several plates developed without ever having been exposed suggest that the explanation for this "edge effect" (41) may be in part that sensitized material is more densely applied to the plates near the edges. Gross fog G, as a function of distance from the plate center, has invariably been found to increase on unexposed plates by an amount between 0.001 and 0.003 density units. Data for a typical sample are plotted in Fig. 17. This observation is compatible with the hypothesis that are thicker near plate edges, although possible effects of nonuniform development or of absorbed moisture have not been evaluated in connection with the edge effect.

The total optical density D_t, including gross fog, of an ideal

Fig. 17. Gross fog as a function of distance from the center for a typical Kodak Process Plate developed in Kodak D-11

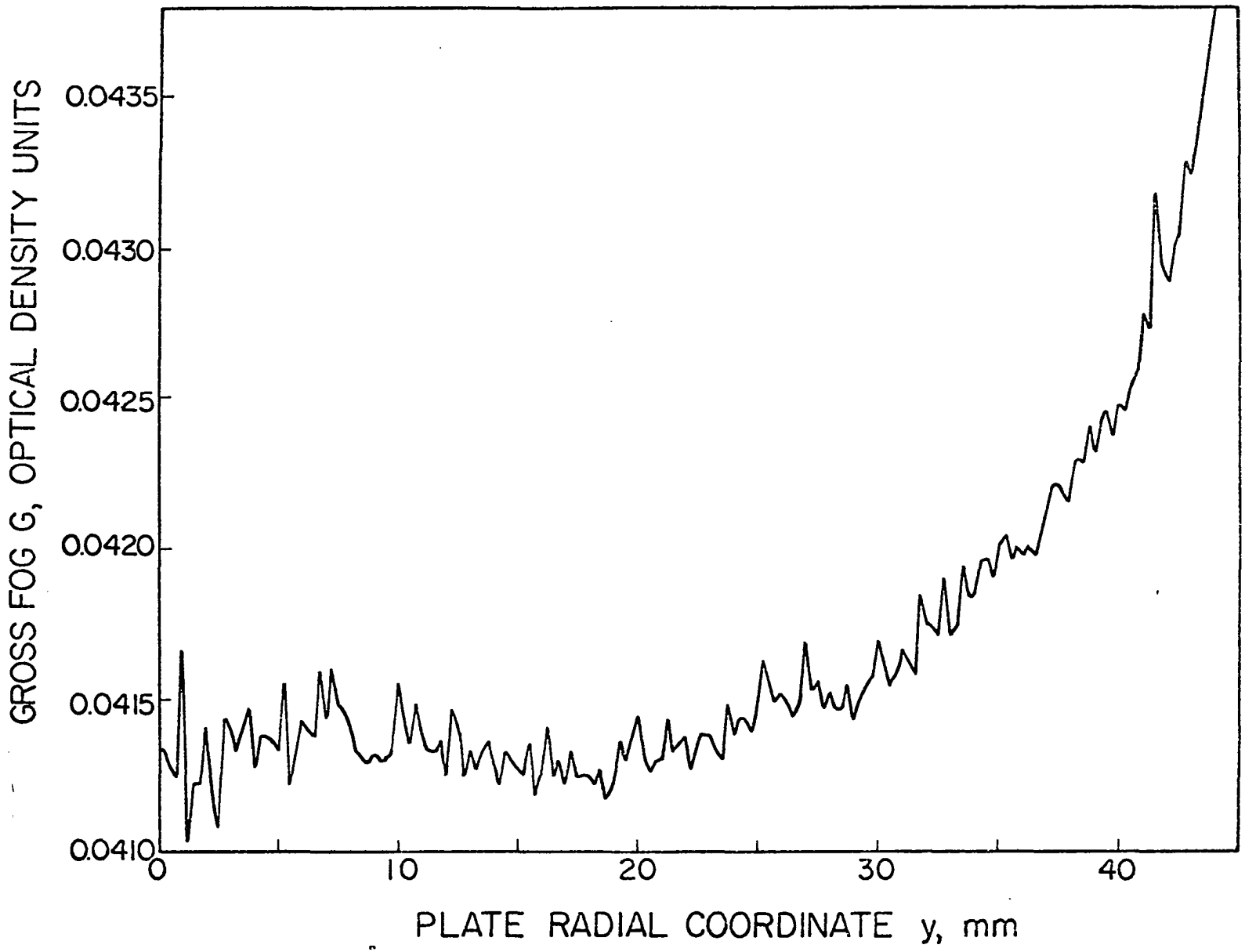
GROSS FOG G, OPTICAL DENSITY UNITS
0.0435
0.0430
0.0425
0.0420
0.0415
0.0410
0
10
20
30
40
PLATE RADIAL COORDINATE y, mm

uniformly exposed plate should be given by

$$D_t^{ideal} = G^\circ + D, \tag{37}$$

where D is the image density, or net darkening due to exposure, of interest and G° is a constant usually between 0.035 and 0.055. Actually, the total may be written as

$$D_t^{actual} = G^\circ p_G + Dp_I, \tag{37'}$$

where G° is the gross fog in the central area of the plate wherein emulsion sensitivity may be regarded as constant, and p_G and p_I are functions of plate radial coordinate y. The data of Fig. 17, for example, where D = 0, suggest $G^\circ = 0.04134$ and

$$\begin{cases} p_G = 1 & y \leq 24 \text{ mm} \\ \\ \simeq 1 + 1.49(10^{-4})(y - 24)^2 & y > 24 \text{ mm}. \end{cases} \tag{38}$$

In practice the function p(y) defined as $(D_t - G^\circ)/D$ can be conveniently observed (39) using uniformly exposed plates, on each of which the corrected image density is know to be a constant $D = D_t^\circ - G^\circ$, where the superscript zeros refer to the central uniformly-sensitive region of a plate. Corrected image densities of working plates are thereafter taken as

$$D = (D_t - G^\circ)/p. \tag{39}$$

For practical purposes the difference $(G^\circ/D)(p_G - 1)$ between p and p_I is less than the uncertainty with which p itself is established. Furthermore, D_t data for a single uniformly exposed plate cannot be separated into $G^\circ p_G$ and Dp_I components, and variation of $G = G^\circ p_G$ curves among unexposed plates is sufficient that such curves are not transferable with enough confidence to make worthwhile the attempted use of the more rigorous correction scheme

$$D = (D_t - G^\circ p_G)/p_I \tag{39'}$$

in place of the simpler scheme outlined above.

2. Density-exposure calibration

A procedure used by Bartell and Brockway (69) to calibrate the dependence of optical density D on electron exposure E led to expression of the ratio E/D as a function

$$F(D) = 1 + cD. \tag{40}$$

A value near 0.3 was indicated (69) for the constant c in the case of Eastman Contrast Lantern Slide Plates. Controversy (70,71) over the validity of this result for the region of densities less than about 0.5 went partially unresolved because of experimental limitations: Density and exposure data with very small uncertainties are necessary for accurate assessment of small deviations from linearity in the emulsion response. Indications were subsequently obtained by a different calibration procedure (33, Footnote 5) that the nonlinearity of Kodak Process Plates was even smaller, corresponding to $c = 0.05 \pm 0.01$ in the above expression for F(D). Inconsistent results were obtained (72, Footnote 6; 73) in attempts to verify this result for low densities by the earlier method (69) of calibration. Kimura and Kimura (74), meanwhile, developed a procedure which, when applied to Fuji Process Hard Plates, yielded a calibration which is shown in Fig. 18. For the most part (*i. e.*, for $0.22 < D < 1.00$) this function lies between the lines $F(D) = 1 + 0.05D$ (- — - — -) and $F(D) = 1 + 0.3D$ (•••••), and is plausible in that respect. It is not to be presumed valid for densities above 0.74 (dashed portion in Fig. 18), which is the upper limit of density data from which the curve was derived. The form of the Kimura function is of doubtful utility for an extended density range,

Fig. 18. Comparison of emulsion calibration functions.
(•••••) Eastman Contrast Lantern Slide Plates, Ref. 69
(- — - — -) Kodak Process Plates, Ref. 33
(—— ---) Fuji Process Hard Plates, Ref. 74; dashed portion is extrapolation
(———) Kodak Process Plates, this work

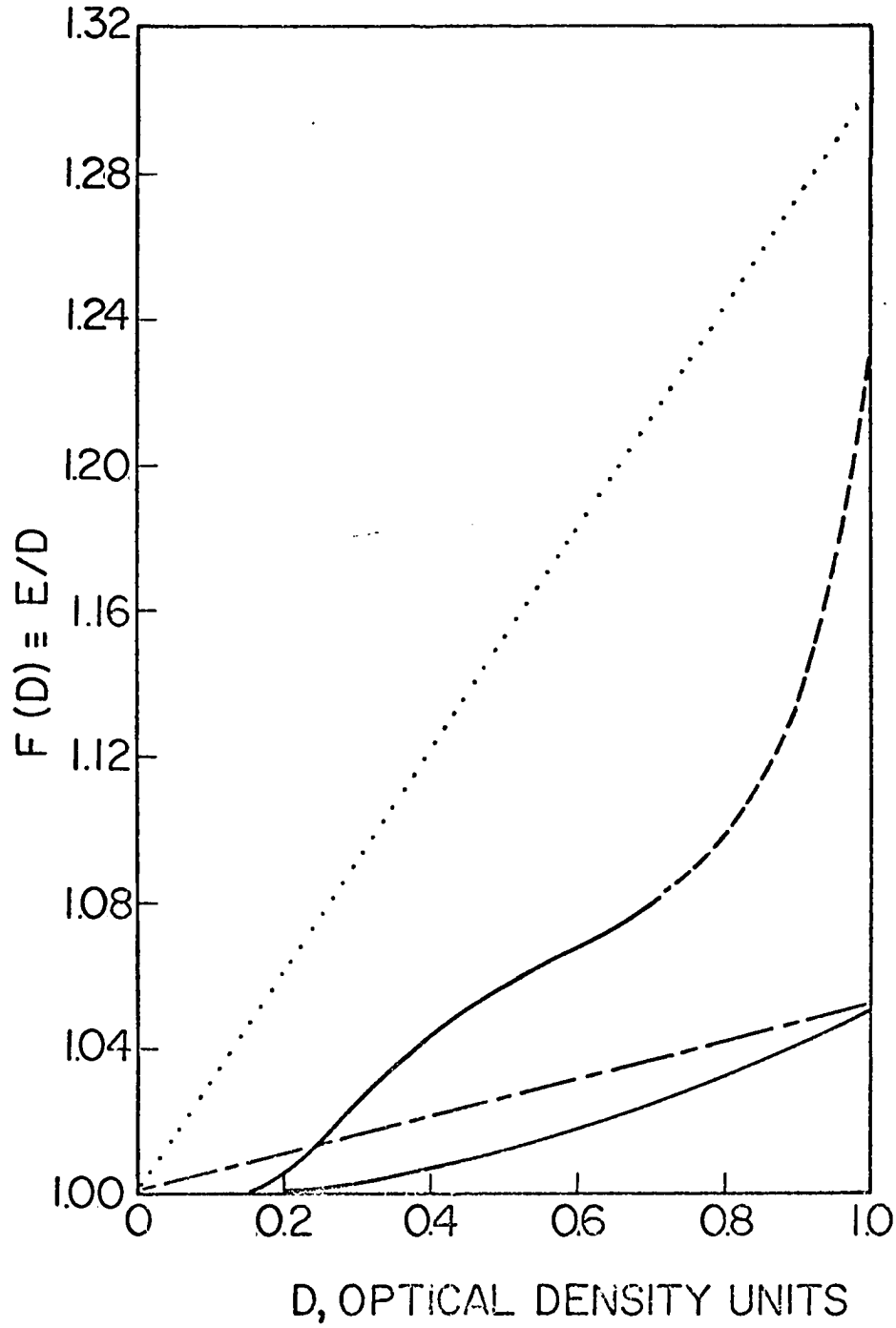
1.32
1.28
1.24
1.20
1.16
1.12
1.08
1.04
1.00
F (D) ≡ E/D
0
0.2
0.4
0.6
0.8
1.0
D, OPTICAL DENSITY UNITS

because the implied density correction increases very rapidly with density above 1.0. Early attempts in this laboratory to adapt the direct least-squares method of analysis to Kodak Process Plate data covering a wide range of densities failed because of the same experimental limitations encountered in applying the method of Bartell and Brockway to the same data. Workable results, however, have been obtained in the investigation to be outlined below, in which a new computer program, incorporating methods devised to circumvent the calibration difficulties encountered previously, was developed for treating calibration data.

The method used here depends on the same essential assumption of exposure pattern similarity for replicate plates taken under experimental conditions identical except for varying exposure duration relied upon by others (69,74,75). Direct nonlinear least-squares optimization of the constant parameters of a calibration function, as suggested by Kimura and Kimura (74), avoids the possible accumulation of errors which they mention and is a more straightforward method than that of Ref. 69. More importantly, it is also more readily adaptable and convenient to use in experimentation with various mathematical models, and was therefore adopted in the present study.

Suppose there are documented as functions of plate radial coordinate y the optical density patterns $D_1(y)$ and $D_2(y)$ for two electron diffraction plates 1 and 2 taken under identical circumstances, except that the exposure time for plate 2 is appreciably less than that for plate 1, so that the observable density ratio function

$$Q(y) \equiv D_2(y)/D_1(y) \tag{41}$$

is everywhere significantly less than unity. If the corresponding exposure patterns are $E_1(y)$ and $E_2(y)$, then the ratio

$$Q_E \equiv E_2(y)/E_1(y) \tag{42}$$

should be a constant equal to the ratio of the exposure times. It is therefore assumed that there is some function $\varepsilon(D)$ of density which involves a set $\vec{\alpha}$ of constant parameters $\alpha_1, \alpha_2, \ldots$ and which gives the exposure:

$$E(y) = \varepsilon[D(y)]. \tag{43}$$

It should then be possible to determine the elements of $\vec{\alpha}$ by minimizing the quantity

$$s(\vec{\alpha}) = \sum\{[\varepsilon(D_2)/\varepsilon(D_1)] - Q_E\}^2 \tag{44}$$

with respect to the calibration constants $\alpha_1, \alpha_2, \ldots$ using a Gauss-Newton least squares technique, once an appropriate functional form is chosen for ε. In practice, there are several additional considerations which enter into a successful determination of a calibration curve.

First, even though exposure times can be measured with six-figure precision, the value of the true exposure ratio Q_E is not known with corresponding accuracy because both the electron beam intensity and concentration of scattering material can fluctuate during and between exposures. Without accurate experimental knowledge of the exposure ratio, therefore, it is necessary to allow the constant Q_E to vary in the least-squares iteration process along with the elements of $\vec{\alpha}$. This constant interacts to some extent with the other variables in the minimization of $s(\vec{\alpha})$ because the exact form of the function ε is not known. The determination of the constants of ε is therefore uncertain to the extent that the ratio $\varepsilon(D_2)/\varepsilon(D_1)$ is being fitted to an incorrect Q_E.

If the emulsions are indeed not very seriously nonlinear in the region of small D, and if saturation (69) or coincidence losses are responsible for whatever nonlinearity appears at higher D values, then the function ε ought to be such that it meets the following criterion in order to be considered acceptable:

(a) $F(D) \equiv \varepsilon(D)/D$ should be a rather mild, smooth, nondecreasing function of D such that $\lim_{D \to 0+} F(D) = b$, where b is an arbitrary scale factor which is always taken as unity.

The condition (a) on ε leads for the observable density ratio curves $Q(D_1)$ to the additional expectations that:

(b) $Q(D_1)$ should also be a mild, smooth, nondecreasing function of D_1;

and

(c) $\lim_{D_1 \to 0+} Q(D_1) = Q_E$.

$Q(D_1)$ data covering an adequate range of D_1 were obtained for this study, as in Ref. 69, using a quadratic sector which gave patterns similar to those used by Bartell and Brockway (69, Fig. 1). It proved easy to get smooth, reproducible $Q(D_1)$ curves with only the residual gas at a steady-state pressure reached after prolonged pumping as the scattering material in the diffraction chamber. Density data were taken from within 30 mm of plate centers to avoid complications due to the edge effect discussed earlier. The role of gross fog, however, was found to be critical in determining the shape of experimental Q curves, and small errors ΔG in G are sufficient to cause density ratio observations to fail to satisfy (b) and (c) above. Subtraction from a total density D_t a gross fog value G which is in error by

an amount ΔG leads to an observed ratio curve

$$Q(D_1) = [D(y) + \Delta G]_2/[D(y) + \Delta G]_1 \qquad (45)$$

which is dominated at small values of D_1 by the ratio $(\Delta G)_2/(\Delta G)_1$, not by Q_E. The usual method of determining G, which consists of reading full-scale lamp intensity through a clear portion near the edge of a plate, may be expected to result in a nonzero error[6] ΔG of this sort, as can be seen from the place-to-place variation of G on a single unexposed plate typified by the data of Fig. 17.

This state of affairs can be taken into account by modifying the least-squares calculation to give minimization of

$$s(\vec{\alpha}) = \sum\{[\varepsilon(D_t - G)_2/\varepsilon(D_t - G)_1] - Q_E\}^2 \qquad (44')$$

with respect to $\vec{\alpha}$, G, and Q_E. Output values of G can then be checked for plausibility by seeing whether or not they fall in the known usual range, from 0.035 to 0.055. In practice the least-squares calculation may not converge if G is allowed to vary independently for each plate. Satisfactory results have nevertheless been obtained by assuming that G is the same for all plates in a set, and they suggest that the assumption is within reason.

Results were derived using

$$\varepsilon(D) = D + \alpha D^3 \qquad (22')$$

for the functional form of ε. This is the simplest form which satisfies (a) and is such that F(D) has zero slope at D = 0, as proposed by Karle and Karle (70). A computer program for minimizing $s(\vec{\alpha})$ using data from up to five plates at a time (*i. e.*, varying four Q_E values and one G value

---

[6]This small additive error, which has strong influence in emulsion calibration work, is of essentially no consequence in routine measurements of molecular scattering features.

simultaneously) was used to analyze data which were split into two sets from one group of five plates and a third set of data from an additional pair of plates. The data included densities from 0.10 to 1.7.

Values of α obtained were 0.046_3 from the paired plates, and 0.051_4 and 0.050_6 from the five. The degree of reproducibility here is good, and the function

$$\varepsilon(D) = D + 0.05D^3 \tag{22}$$

satisfies (a), p. 97. Reasonable Q_E and G values were also obtined, and in cross-checking it was verified that the G's could be used to reconstruct image density ratio curves satisfying (b) and (c). Residual rms noise results, proportional to $\sqrt{s_{min}}$, were comparable with the level of reproducibility usually obtainable in $D_t(y)$ patterns on replicate plates taken with identical exposure times.

Calculations made to test the alternative model (33,69) $\varepsilon(D) = D + cD^2$ corresponding to Eq. 40 resulted in $\sqrt{s_{min}}$ values two to three times larger than did the $D + \alpha D^3$ trials, although for α and c near 0.05 the difference in density corrections implied by these two alternatives hardly matters.

On the basis of the results derived, it is believed that for $0 < D < 1.5$ the function $F(D) = 1 + 0.05D^2$ represents the response of Kodak Process Plate emulsions to exposure with 40 kV electrons about as well as can be ascertained using data presently available. Conclusive confirmation of this result would require data in which the uncertainties of Q_E and G did not exist so that these quantities could be held fixed in the least-squares computation. The general method of analysis itself, however, should be applicable to such improved data, and the results already ob-

tained make it seem unlikely that further investigation should yield emulsion calibration functions grossly different[7] from Eq. 22 for Process Plates given comparable exposure and development.

---

[7]One possible improvement might be to take

$$\begin{cases} F(D) = D & D \leq d \\ = D + \alpha(D - d)^3 & D > d, \end{cases}$$

where d is some optimally chosen constant value, probably between 0.4 and 0.9. This possibility has not been investigated here.

LITERATURE CITED

1. J. W. Mallet, Am. Chem. J. 3, 189 (1881).

2. T. E. Thorpe and F. J. Hambly, J. Chem. Soc. 55, 163 (1889).

3. J. Simons and J. H. Hildebrand, J. Am. Chem. Soc. 46, 2183 (1924).

4. K. Fredenhagen, Z. Anorg. Allgem. Chem. 210, 210 (1933); 218, 161 (1934).

5. G. Briegleb, Naturwiss. 29, 420 (1941).

6. G. Briegleb, Z. Physik. Chem. (Leipzig) Abt. B 51, 9 (1941); 52, 368 (1942).

7. R. W. Long, J. H. Hildebrand, and W. E. Morrell, J. Am. Chem. Soc. 65, 182 (1943).

8. R. L. Jarry and W. Davis, Jr., J. Phys. Chem. 57, 600 (1953).

9. W. Strohmeier and G. Briegleb, Z. Elektrochem. 57, 662 (1953).

10. S. H. Bauer, J. Y. Beach, and J. H. Simons, J. Am. Chem. Soc. 61, 19 (1939).

11. R. A. Oriani and C. P. Smyth, *ibid.* 70, 125 (1948).

12. D. W. Magnuson, Microwave dielectric constant measurements on hydrogen fluoride vapor (Report K-1180, Union Carbide Corporation Nuclear Division, Oak Ridge, Tenn., 1954).

13. D. F. Smith, J. Chem. Phys. 28, 1040 (1958).

14. J. Hu, D. White, and H. L. Johnston, J. Am. Chem. Soc. 75, 1232 (1953).

15. E. U. Franck and W. Spalthoff, Naturwiss. 40, 580 (1953).

16. E. U. Franck and W. Spalthoff, Z. Elektrochem. 61, 348 (1957).

17. W. Spalthoff and E. U. Franck, *ibid.* 61, 993 (1957).

18. E. U. Franck and F. Meyer, *ibid.* 63, 571 (1959).

19. E. U. Franck, *ibid.* 57, 674 (1953).

20. J. N. Butler and R. S. Brokaw, J. Chem. Phys. 26, 1636 (1957).

21. J. W. Armitage, P. Gray, and P. G. Wright, J. Chem. Soc. 1963, 1796.

22. G. Briegleb and W. Strohmeier, Z. Elektrochem. 57, 668 (1953).

23. J. N. Maclean, F. J. C. Rossotti, and H. S. Rossotti, J. Inorg. Nucl. Chem. 24, 1549 (1962).

24. D. F. Smith, J. Mol. Spectry. 3, 473 (1959).

25. F. J. C. Rossotti and H. Rossotti, J. Phys. Chem. 65, 926, 930, 1376 (1961).

26. E. A. Guggenheim, *Mixtures* (Oxford University Press, London, 1952).

27. G. N. Lewis, M. Randall, K. S. Pitzer, and L. Brewer, *Thermodynamics* (McGraw-Hill Book Company, Inc., New York, 1961), 2nd ed.

28. J. Simons, J. Am. Chem. Soc. 46, 2179 (1924).

29. H. H. Hyman and J. J. Katz, in *Non-aqueous solvent systems*, T. C. Waddington, Ed. (Academic Press, Inc., New York, 1965).

30. M. Atoji and W. N. Lipscomb, Acta Cryst. 7, 173 (1954).

31. E. Safary, J. Romand, and B. Vodar, J. Chem. Phys. 19, 379 (1951).

32. D. K. Hindermann and C. D. Cornwell, *ibid.* 48, 2017 (1968).

33. L. S. Bartell, K. Kuchitsu, and R. J. deNeui, *ibid.* 35, 1211 (1961).

34. B. L. Carroll (unpublished Ph. D. thesis, Iowa State University, Ames, Iowa, 1963).

35. J. P. Guillory (unpublished Ph. D. thesis, Iowa State University, Ames, Iowa, 1965).

36. S. Shibata and L. S. Bartell, J. Chem. Phys. 42, 1147 (1965).

37. L. S. Bartell and L. O. Brockway, Phys. Rev. 90, 833 (1953).

38. L. S. Bartell, D. A. Kohl, B. L. Carroll, and R. M. Gavin, Jr., J. Chem. Phys. 42, 3079 (1965).

39. D. J. Dahm, Nonuniform densities on uniformly exposed Kodak Process Plates (personal communication, Ames, Iowa, 1965).

40. D. A. Kohl and R. A. Bonham, J. Chem. Phys. 47, 1634 (1967).

41. D. A. Kohl (unpublished Ph. D. thesis, Indiana University, Bloomington, Indiana, 1966).

42. L. S. Bartell, J. Appl. Phys. 31, 252 (1960).

43. L. S. Bartell and H. K. Higginbotham, J. Chem. Phys. 42, 851 (1965).

44. L. S. Bartell and J. P. Guillory, *ibid.* 43, 647 (1965).

45. R. A. Bonham and L. S. Bartell, *ibid.* 31, 702 (1959).

46. R. A. Bonham and T. Ukaji, *ibid.* 36, 72 (1962).

47. B. B. Howard, *ibid.* 39, 2524 (1963).

48. Y. Morino, S. J. Cyvin, K. Kuchitsu, and T. Iijima, *ibid.* 36, 1109 (1962).

49. Y. Morino, K. Kuchitsu, and M. Tanimoto, Electron diffraction study of carbon suboxide (approximate title, to be published).

50. K. Kuchitsu and L. S. Bartell, J. Chem. Phys. 35, 1945 (1961).

51. G. Herzberg, *Spectra of diatomic molecules* (D. Van Nostrand Company, Inc., Princeton, N. J., 1950), 2nd ed., p. 536.

52. R. H. Hughes, R. J. Martin, and N. D. Coggeshall, J. Chem. Phys. 24, 489 (1956).

53. D. Hadži, Ed., *Hydrogen bonding* (Pergamon Press, Inc., New York, 1959).

54. J. S. Kittelberger and D. F. Hornig, J. Chem. Phys. 46, 3099 (1967).

55. F. Seel, W. Birnkraut, and D. Werner, Chem. Ber. 95, 1264 (1962).

56. F. Seel (personal communication to L. S. Bartell, Saarbrücken, Germany, 1964).

57. R. S. Siegel, Products of the reaction between liquid nitrosyl chloride and hydrogen fluoride (unpublished manuscript BNL 7735, Brookhaven National Laboratory, Upton, N. Y., 1964).

58. J. Kleinberg, W. J. Argersinger, Jr., and E. Griswold, *Inorganic Chemistry* (D. C. Heath and Company, Boston, Mass., 1960), p. 398.

59. D. W. Magnuson, J. Chem. Phys. 19, 1071 (1951).

60. D. W. Magnuson, Phys. Rev. 83, 485 (1951).

61. K. Venkateswarlu and S. Mariam, Proc. Indian Acad. Sci. Sect. A 61, 260 (1965).

62. L. H. Jones, L. B. Asprey, and R. R. Ryan, J. Chem. Phys. 47, 3371 (1967).

63. L. S. Bartell and K. Kuchitsu, J. Phys. Soc. Japan 17, Supplement B-II, 20 (1962).

64. K. Hedberg, Trans. Am. Crystallographic Assoc. 2, 79 (1966).

65. Y. Morino, K. Kuchitsu, and T. Fukuyama, Bull. Chem. Soc. Japan 40, 423 (1967).

66. D. A. Kohl, *loc. cit.*, Chap. IV.

67. R. A. Day, Jr. and A. L. Underwood, *Quantitative analysis* (Prentice-Hall, Inc., Englewood Cliffs, N. J., 1958), pp. 389-390, 414.

68. Eastman Kodak Company, Kodak plates and films for science and industry (Kodak publication P-9, Rochester, N. Y., 1967), 3rd printing.

69. L. S. Bartell and L. O. Brockway, J. Appl. Phys. 24, 656 (1953).

70. I. L. Karle and J. Karle, *ibid.* 24, 1522 (1953).

71. L. S. Bartell and L. O. Brockway, *ibid.* 24, 1523 (1953).

72. H. K. Higginbotham and L. S. Bartell, J. Chem. Phys. 42, 1131 (1965).

73. K. W. Hansen and L. S. Bartell, Inorg. Chem. 4, 1775 (1965).

74. K. Kimura and M. Kimura, J. Chem. Phys. 32, 1398 (1960).

75. J. Karle and I. L. Karle, *ibid.* 18, 957 (1950).

ACKNOWLEDGEMENTS

The author gratefully acknowledges the patient guidance and supervision given generously to this work by Prof. L. S. Bartell. Financial support, as teaching and research assistantships, was provided during the author's graduate studies by Iowa State University, The Ames Laboratory of the U. S. Atomic Energy Commission, The University of Michigan, and the National Science Foundation.

Thanks are due to numerous graduate students and postdoctoral fellows, past and present, of Dr. Bartell's research group for many helpful discussions and suggestions, but especially to Mrs. Kathryn W. Hansen, Dr. Jack P. Guillory, and Dr. Harlan K. Higginbotham for valuable instruction in techniques of operating the diffraction apparatus. A four-year association with Dr. H. Bradford Thompson has also been quite stimulating.

And to my wife, who deserves it the most, my gratitude is too great to express except to her.